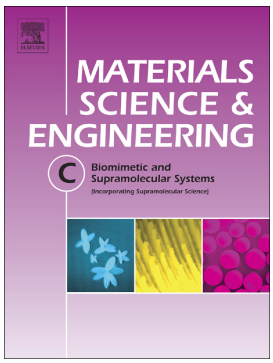

Anticancer prospects of silver nanoparticles green-synthesized by plant extracts

Eun-Young Ahn, Youmie Park

PII: S0928-4931(20)30311-8

DOI: https://doi.org/10.1016/j.msec.2020.111253

Reference: MSC 111253

To appear in: *Materials Science & Engineering C*

Received date: 22 January 2020

Revised date: 15 June 2020

Accepted date: 30 June 2020

Please cite this article as: E.-Y. Ahn and Y. Park, Anticancer prospects of silver nanoparticles green-synthesized by plant extracts, *Materials Science & Engineering C* (2020), https://doi.org/10.1016/j.msec.2020.111253

2020.6.15.

Anticancer prospects of silver nanoparticles green-synthesized by plant extracts

Eun-Young Ahn and Youmie Park*

College of Pharmacy and Inje Institute of Pharmaceutical Sciences and Research, Inje University, 197 Inje-ro, Gimhae, Gyeongnam 50834, Republic of Korea

*To whom correspondence should be addressed.

Youmie Park, Professor, Ph.D.

email: youmiep@inje.ac.kr; phone: +82-55-320-3884

Revised for *Materials Science & Engineering C Materials for Biological Applications*

June 2020

Graphical Abstract

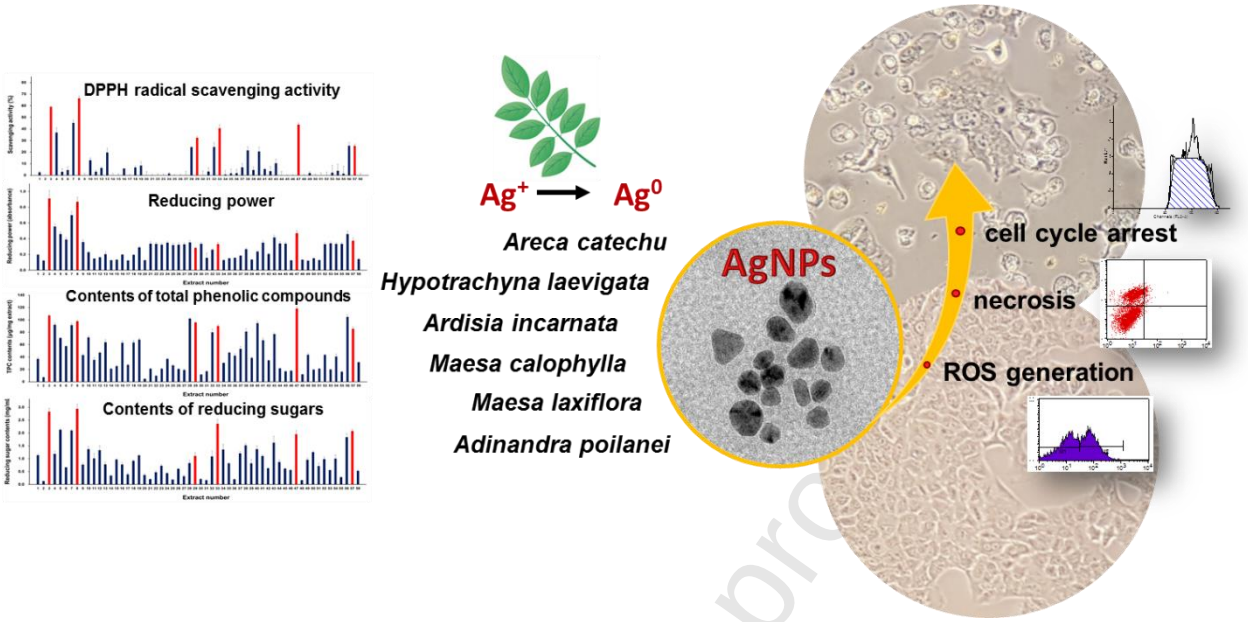

Abstract

Silver nanoparticles (AgNPs) were synthesized *via* a green strategy using fifty-eight plant extracts that originated from Vietnam and Indonesia. Among the fifty-eight AgNP samples, we selected six AgNP samples synthesized by the extracts of *Areca catechu*, *Hypotrachyna laevigata*, *Ardisia incarnata*, *Maesa calophylla*, *Maesa laxiflora* and *Adinandra poilanei*. Remarkably, these six extracts exhibited higher 2,2-diphenyl-1-picrylhydrazyl radical scavenging activity and reducing power than the other extracts. Furthermore, the contents of total phenolic compounds and reducing sugars in the six selected extracts were also higher than those in the other extracts. The six selected AgNP samples showed strong surface plasmon resonance in the range of 416 ~ 438 nm. They were all spherical shaped with an average size from 12.5 ± 1.0 nm to 21.3 ± 4.9 nm as measured by field-emission transmission electron microscopy images. The hydrodynamic sizes were measured to be 49.5 ~ 122.6 nm with negative zeta potential values. Colloidal stability was excellent on the shelf for 28 days and in cell culture medium. The cytotoxicity assessment and generation of reactive oxygen species (ROS) in A549 and HeLa cells demonstrated that the AgNP samples prepared by *Ardisia incarnata*, *Maesa calophylla*, and *Maesa laxiflora* showed relatively high cytotoxicity and excess ROS generation among the six selected AgNP samples. Exposure of the AgNP samples to A549 and HeLa cells resulted in cell death, which was mostly due to necrosis but slightly due to late apoptosis. Cell cycle analysis demonstrated a significant increase in the cell population in the S phase. The green-synthesized AgNPs induced cell death, suggesting anticancer prospects that may offer new insight into the development of an anticancer nanomedicine.

Keywords: green synthesis; silver nanoparticles; cytotoxicity; reactive oxygen species; necrosis, apoptosis; cell cycle

1. Introduction

The conventional practices of cancer treatment are surgery, chemotherapy and radiation therapy [1]. Emerging nanotechnology has gained substantial interest in overcoming some of the side effects of conventional cancer therapy [2,3]. Nanosized materials have unique physical and chemical properties. Specifically, silver nanoparticles (AgNPs) have drawn the attention of researchers owing to their beneficial biological activities, including antimicrobial, wound healing and anticancer activities [4]. Currently, a green synthetic method is preferred for the synthesis of AgNPs. Diverse natural products have been used as green reductants to reduce Ag ions to AgNPs [5,6]. Among natural products, plant extracts are frequently selected due to their advantages of environmental friendliness and cost effectiveness [4,7]. It has been reported that plant metabolites such as terpenoids, phenolics, flavonoids, alkaloids and polysaccharides contribute to the reduction of Ag ions to AgNPs [8]. Plant extracts possess their own biological activities that are beneficial to human health. When plant extracts are used for synthesis, the resulting AgNPs exert synergistic activities by combining the activities of both materials (the plant extracts and the AgNPs). Excellent reviews regarding the green synthesis of AgNPs using plant extracts can be found elsewhere [8-11]. The reducing power of plant extracts allows the nucleation of Ag ions and further affects the growth and colloidal stability of AgNPs [12]. Subramanian et al. reported that the reducing power of plant extracts depends on the amount of water-soluble phenolic compounds, which play an important role in the reduction of Ag ions [13]. Furthermore, the size, morphology and stability of metallic nanoparticles depend on the method of preparation, nature of the solvent, mixing ratio, concentration, pH and temperature of the reaction mixture and the strength of the reducing agent [8,14,15].

The cytotoxicities of metallic nanoparticles synthesized by plant extracts is well reviewed elsewhere [16,17,18]. The cytotoxicity of plant-mediated metallic nanoparticles is dependent on the time and dose. Furthermore, cytotoxicity is affected by the size and shape of the nanoparticles.

Smaller nanoparticles show higher cytotoxicity, and spherical nanoparticles are more potent than other shapes [19,20]. When the same plant was used for the synthesis of gold nanoparticles (AuNPs) and AgNPs, the resulting AgNPs were more cytotoxic than the resulting AuNPs regardless of the cancer cells tested. The cytotoxicity of AgNPs is closely associated with reactive oxygen species (ROS) generation [21].

The purpose of the current report is the green synthesis of AgNPs using fifty-eight extracts that originated from Vietnam and Indonesia. The following factors were measured for each extract to determine the relationship between these factors and the synthetic trends of AgNPs: 2,2-diphenyl-1-picrylhydrazyl (DPPH) radical scavenging activity, reducing power, and contents of total phenolic compounds and reducing sugars. Among the fifty-eight AgNP samples, six samples were selected for further study. The synthetic yields were estimated by inductively coupled plasma mass spectrometry (ICP-MS). Field emission transmission electron microscopy (FE-TEM) was utilized to obtain information about the shape and size of the nanoparticles. Colloidal stability on the shelf was assessed using UV-visible spectrophotometry. Hydrodynamic size and zeta potential measurements were performed, and the cytotoxicity was evaluated in A549 (human lung carcinoma) and HeLa (human epithelial cervix adenocarcinoma) cells upon treatment with the six selected AgNP samples. ROS generation, apoptosis/necrosis induction by Annexin V/PI staining and cell cycle analysis were also investigated to explore the potential applications of the six selected AgNP samples as anticancer agents.

2. **Materials and methods**

2.1. Materials

Fifty-eight plant extracts grown in Vietnam and Indonesia were purchased from the International Biological Material Research Center (Daejeon, Republic of Korea). Table 1 provides information on the fifty-eight plant extracts that were used in the current report. Gallic acid, Folin–Ciocalteu's reagent, potassium sodium tartrate, potassium persulfate, silver nitrate, sodium phosphate dibasic, sodium phosphate monobasic, trichloroacetic acid, sodium carbonate, sodium bicarbonate, sodium sulfate, copper sulfate pentahydrate, hexaammonium heptamolybdate tetrahydrate, and disodium hydrogen arsenate heptahydrate were obtained from Sigma-Aldrich (St. Louis, MO, USA). DPPH was obtained from Alfa Aesar (Ward Hill, MA, USA). Iron(III) chloride and sulfuric acid were obtained from Duksan (Gyeong-gi, Republic of Korea). Potassium hexacyanoferrate(III) was obtained from Wako (Osaka, Japan). High-glucose Dulbecco's modified Eagle's medium (DMEM, with sodium pyruvate), fatal bovine serum (FBS), penicillin, streptomycin, trypsin-EDTA, and phosphate-buffered saline (PBS) were purchased from Gibco BRL (Grand Island, NY, USA). The EZ-CYTOX assay kit to check cell viability was obtained from DoGenBio (Gyonggi, Republic of Korea). The Annexin V-FITC (fluorescein isothiocyanate) apoptosis detection kit I and PI/RNase staining buffer were purchased from BD Biosciences (San Jose, CA, USA). H_2DCFDA (2',7'-dichlorodihydrofluorescein diacetate), obtained from Thermo Fisher Scientific (Scoresby, VIC, Australia), was used for ROS detection.

2.2. Instruments

UV-visible spectra were acquired using a Shimadzu UV-2600 spectrophotometer (Shimadzu Corporation, Kyoto, Japan). FE-TEM images were obtained by using a JEM-2100F (JEOL, Tokyo, Japan). Hydrodynamic size and zeta potential values were measured with a NanoBrook 90 Plus Zeta analyzer (Brookhaven Instruments Corporation, Holtsville, NY, USA). The reaction yields of the AgNPs were assessed with a Thermo Fisher Scientific iCAP TQ ICP-MS (Bremen, Germany). The

absorbance of 96-well microplates was measured by the Synergy HT multidetection microplate reader and by Cytation 5 (BioTek Instruments, VT, USA).

2.3. Preparation of the extracts

Fifty-eight plant extracts (Table 1) were supplied by the Foreign Plant Extract Bank (Daejeon, Republic of Korea). For preparation of the Vietnamese plant extracts, each dried and refined plant (100 g) was extracted with 600 mL of methanol (99.9%) with sonication for three days at 45 °C. During extraction, sonication was performed for 15 min followed by resting time for 2 h. This process was repeated for three days. The resulting extract was filtered through nonfluorescent cotton and concentrated with a rotary evaporator under reduced pressure at 45 °C. Then, the residual solvent was removed by freeze-drying to obtain the methanol extract of the Vietnamese plants. For preparation of the Indonesian plant extracts, after drying and grinding each plant, the plant powder (150 g) was extracted by maceration at ambient temperature for 18 h with 150 mL of ethanol (aqueous, 95%) or methanol (99.9%). The extract was filtered to remove the insolubles, and the filtrate was concentrated with a rotary evaporator (Laborota 4000, Heidolph, Jakarta, Indonesia) under reduced pressure to obtain the extracts of the Indonesian plants. For the green synthesis in the following section, the fifty-eight extracts prepared from the Vietnamese and Indonesian plants above were dissolved in 50% ethanol to a final concentration of 2%. These solutions were then filtered through a nylon syringe filter (0.2 μm, Agilent Technologies, Lake Forest, CA, USA). Then, the filtrate was stored at -20 °C prior to use.

2.4. Green synthesis of the AgNPs

A mixture of $AgNO_3$ (final concentration, 0.25 mM) and three different concentrations of the extracts (final concentrations of 0.005%, 0.01% and 0.02%) were prepared in a total volume of 1 mL, and the mixture was vortexed for 10 s. Then, the mixture was reacted in a 37 °C shaking water bath at 170 rpm. After a 24 h of incubation, the reaction was terminated by cooling in a 5 °C refrigerator for 10 min. Then, UV-visible spectra were acquired from 300 to 900 nm using a multidetection microplate reader. The colloidal solution of AgNPs was named after the extract number in Table 1. When plant extract number 1 was used for the synthesis, the resulting AgNPs were named AgNPs-1.

2.5. *DPPH radical scavenging activity of the fifty-eight extracts*

The DPPH radical scavenging activity of the fifty-eight extracts was carried out according to a previous method [12]. The 2% concentration of the fifty-eight plant extracts was diluted to 0.02% by adding deionized water. The diluted extract (0.02%) was used to assess the DPPH radical scavenging activity. Thirty microliters of the diluted extract (0.02%) was mixed with DPPH radical solution (0.1 mM, 170 μL), and the mixture was incubated at ambient temperature for 30 min. Then, the absorbance at 517 nm was measured with a multidetection microplate reader. An aqueous solution of ethanol (50%) was used as a blank instead of the plant extract. All experiments were performed in triplicate.

2.6. *Reducing power of the fifty-eight extracts*

The reducing power of the fifty-eight extracts was determined according to a previous report [12]. One hundred microliters of each of the following three solutions was mixed and incubated in a dry oven at 50 °C: plant extract (0.02%), phosphate buffer (0.2 M, pH 6.6) and potassium hexacyanoferrate(III) (1%). After 20 min of incubation, the reaction mixture was quickly cooled to

ambient temperature, and trichloroacetic acid (10%, 300 μL) was added. Then, the mixture was centrifuged at 3,400 ×*g* for 10 min. Next, the supernatant (500 μL) was recovered, and 0.1% iron(III) chloride solution (100 μL) was added to the supernatant. After 10 min of incubation, the absorbance at 700 nm was measured with a multidetection microplate reader. All experiments were performed in triplicate.

2.7. Total phenolic compound (TPC) content of the fifty-eight extracts

The TPC content of the fifty-eight extracts was determined according to a previously described method [22]. One hundred microliters of the extract (0.02%) was added to a mixture of 2 M Folin–Ciocalteu's reagent (50 μL), 20% Na_2CO_3 (150 μL) and deionized water (500 μL). The absorbance at 765 nm was measured after 1 h of incubation at ambient temperature. The TPC contents were expressed as gallic acid (μg) equivalents (GAE) per milligram of extract (μg GAE/mg extract). A standard curve was generated by using gallic acid.

2.8.Reducing sugar content of the fifty-eight extracts

The reducing sugar content of the fifty-eight extracts was determined according to the previously described Nelson-Somogyi method [23]. This method utilizes the reducing properties (in the presence of a potential aldehyde or keto group) of carbohydrates. Nelson's A reagent was composed of sodium carbonate (2.5 g), potassium sodium tartrate (2.5 g), sodium bicarbonate (2.0 g), and sodium sulfate (2.0 g). These four salts were dissolved in 100 mL of distilled water. For Nelson's B reagent, copper sulfate pentahydrate (7.5 g) was dissolved in 50 mL of distilled water, and then one drop of concentrated sulfuric acid was added. Nelson's reagent C was comprised of a mixture of

Nelson's A and B reagents (25:1) and prepared just before use. For Nelson's color reagent, two solutions were prepared as follows: (1) hexaammonium heptamolybdate tetrahydrate (5 g) was dissolved in 80 mL of deionized water, concentrated sulfuric acid (4.2 mL) was added; and (2) disodium hydrogen arsenate (0.6 g) was dissolved in deionized water (5 mL). These two solutions were mixed in a brown-colored bottle, and the final volume was adjusted to 100 mL by adding deionized water. Nelson's color reagent was reacted at 37 °C for 24 h before use. A mixture of the sample (0.5 mL) and Nelson's reagent C (0.5 mL) was reacted in boiling water for 20 min. After cooling to ambient temperature, with Nelson's color reagent (0.5 mL) was added to the mixture followed by incubation at 37 °C for 5 min. The absorbance at 520 nm was measured for each sample. Then, the reducing sugar content was expressed as mg glucose equivalents per milligram of extract (mg glucose/mg extract). Glucose was used as a standard to construct a standard curve.

2.9. Determination of the synthetic yield of the six selected AgNP samples

The synthetic yield of the AgNPs was assessed by using triple quadrupole ICP-MS (iCAP TQ ICP-MS, Thermo Fisher Scientific, Bremen, Germany). The six selected AgNP samples were centrifuged at 18,600 ×*g* for 3 h to recover the supernatant. Both the unreacted Ag ions in the supernatant and the original colloidal solution of AgNPs were submitted for ICP-MS analysis. The synthetic yield was calculated using the following formulae.

Yield (%) = 100 – [concentration of the unreacted Ag / concentration of Ag in the original colloidal solution]×100

2.10. Colloidal stability of the six selected AgNP samples on the shelf

For the assessment of the colloidal stability on the shelf, the six selected AgNP samples (synthesized with a 0.02% extract concentration) were evaluated at ambient temperature in a dark room after 28 days. Changes in UV-visible spectra in the range of 300 to 800 nm were observed at fixed time intervals (0, 1, 2, 5, 7, 14, 21 and 28 days).

2.11. Cell culture and cytotoxicity

A549 and HeLa cells were purchased from the Korean Cell Line Bank (Seoul, Republic of Korea). Cell culture and cytotoxicity assays were conducted according to our previous reports [12,24,25]. Cells were grown in high-glucose DMEM supplemented with 10% FBS, penicillin (100 units/mL) and streptomycin (100 μg/mL). Cells were grown in a 37 °C incubator supplied with 5% CO_2 and cultured while maintaining 80% confluence. For the cytotoxicity assessment, the six selected AgNP samples were evaluated using an EZ-CYTOX cell viability assay kit. Each type of cell was seeded at a concentration of 5.0×10^3 cells/well in 96-well plates with growth medium. After 24 h of incubation, the cells were incubated with each AgNP sample at various concentrations (25 μM, 50 μM and 100 μM based on the Ag concentration). The control was deionized water instead of an AgNP sample. Then, the cells were cultured at 37 °C under a 5% CO_2 atmosphere. After 24 h incubation, the WST reagent (10 μL) was added to each well, and the plate was incubated for an additional 1 h. Next, the absorbance was measured at 460 nm using a multidetection microplate reader. Due to the intrinsic absorbance of the AgNPs at 460 nm, the absorbance from the AgNPs was subtracted from the absorbance of each sample at 460 nm. All experiments were conducted in triplicate.

2.12. Generation of cellular ROS

ROS generation is known as a critical death process in the cytotoxic mechanism of metallic nanoparticles. This oxidative cell damage induces apoptosis/necrosis, DNA damage, cell cycle arrest and inhibition of cell proliferation [26]. 2',7'-Dichlorodihydrofluorescein diacetate (H_2DCFDA) is a nonfluorogenic dye that is cleaved to its derivative, 2',7'-dichlorodihydrofluorescein (H_2DCF), by cellular esterases after cell internalization. H_2DCF is oxidized to 2',7'-dichlorofluorescein (DCF) by intracellular oxidants such as ROS. DCF accumulates in the cell and can be measured by an increase in fluorescence at 530 nm with excitation at 490 nm [27].

A549 and HeLa cells were seeded at a concentration of 3.0×10^5 cells/well in 6-well plates in growth medium. After 24 h of incubation, cells were incubated with each AgNP sample at a concentration of 50 μM (based on the Ag concentration). The control was deionized water instead of a AgNP sample. Then, the cells were cultured at 37 °C under a 5% CO_2 atmosphere. After 24 h of incubation, each cell was collected by trypsinization. The cell pellet was washed three times with Dulbecco's phosphate-buffered saline (pH 7.4). Next, the H_2DCFDA reagent (2 μM, 1 mL) was added to each cell pellet, and further incubation was performed in the dark at ambient temperature for 1 h. The cell pellet was washed with Dulbecco's phosphate-buffered saline (pH 7.4). Next, each cell pellet was analyzed by measuring the fluorescence intensity (FL1-H) with a FACS Calibur flow cytometer (BD Biosciences, San Jose, CA, USA). For each analysis, 10,000 gate events were measured. The results were analyzed by CellQuest software (Becton-Dickinson Instruments, Franklin Lakes, NJ, USA).

2.13. Annexin V/PI staining

The cells (A549 and HeLa cells, 3×10^5 cells/well) were seeded in 6-well plates. After 24 h of incubation, the medium was changed to new medium containing a AgNP colloidal solution (50 μM

based on the Ag concentration). Then, trypsinization was conducted to collect the cells after a further incubation of 24 h. Next, the cells were washed with cold PBS (pH 7.2) and centrifuged. The pellet was resuspended in binding buffer (100 μL). Next, Annexin V-FITC (5 μL) and PI (5 μL) were used for staining for 15 min at ambient temperature in the dark according to the Annexin V-FITC apoptosis detection kit I manual (BD Biosciences). After staining, binding buffer (500 μL) was added. A FACS Calibur flow cytometer (BD Biosciences, San Jose, CA, USA) was utilized to analyze the cells. In each dataset, 10,000 gate events were recorded. CellQuest software (Becton-Dickinson Instruments, Franklin Lakes, NJ, USA) was used to analyze the proportion of cells (%).

2.14. Cell cycle analysis

The cells (A549 and HeLa cells, 3×10^5 cells/well) were seeded in 6-well plates. After 24 h of incubation, the medium was changed to new medium containing each AgNP sample (50 μM, based on the Ag concentration). Then, trypsinization was performed to collect the cells after a further 24 h incubation. The pellet was resuspended in cold ethanol (70%) and stored in the freezer for at least 1 h to facilitate the DNA staining process. Then, the cells were washed with cold PBS (pH 7.2) and centrifuged (3,000 rpm, 5 min). The pellet was resuspended in PI/RNase staining buffer (0.5 mL) and incubated for 30 min at ambient temperature in the dark. The cell cycle distribution was measured using a FACS Calibur flow cytometer (BD Biosciences, San Jose, CA, USA). In each analysis, 10,000 gate events were measured, and the statistical data were plotted as generated by ModFit LT 4.1 software (Verity Software House Inc., Topsham, ME, USA).

3. Results and discussion

3.1. UV-visible spectra of AgNPs synthesized from fifty-eight extracts

Fifty-eight extracts (Table 1) from Vietnam (35 plants) and Indonesia (23 plants) were applied as reducing agents to synthesize AgNPs *via* a green route. In our previous report, we used thirty plant extracts originating from China for the green synthesis of AgNPs, and their antioxidant, cytotoxic, apoptotic and wound healing properties were evaluated [12]. In the current report, diverse plant parts were used, including leaves, twigs, fruits, roots, barks, flowers, stems and whole plants. The extract concentration varied (0.005%, 0.01% and 002%) during the synthesis, and the resulting UV-visible spectra are displayed in Figure 1. Among the fifty-eight extracts, we selected six AgNP samples with absorbance values greater than 1.0 at the maximum wavelength for further study of colloidal stability, FE-TEM characterization, cytotoxicity, ROS generation and cell cycle analysis. In addition, the synthetic yield, hydrodynamic size and zeta potential were determined. The following six selected AgNP samples showed a relatively high absorbance in the range of 400 ~ 500 nm among the fifty-eight AgNP samples: AgNPs-3 (*Areca catechu*), AgNPs-8 (*Hypotrachyna laevigata*), AgNPs-29 (*Ardisia incarnata*), AgNPs-33 (*Maesa calophylla*), AgNPs-47 (*Maesa laxiflora*) and AgNPs-57 (*Adinandra poilanei*). The extract number was used for labeling the corresponding AgNP samples. For example, when extract 1 was used for the synthesis, the resulting AgNPs were labeled AgNPs-1. The reaction yields of the six selected AgNP samples was estimated by triple quadrupole ICP-MS, and the results are shown in Table 2. The reaction yields were in the range of 91.6 ~ 99.9%, suggesting that the current reaction conditions were optimal to synthesize AgNPs.

3.2. DPPH radical scavenging activity and reducing power of the fifty-eight extracts

We proposed in a previous report that the DPPH radical scavenging activity and reducing power of the extract influenced the green synthesis of AgNPs [12]. The scavenging activity of the six selected

extracts was relatively high and resulted in the successful synthesis of AgNPs (Figure 2). The scavenging activity (%) of each extract was as follows: 3 (59.0%), 8 (66.4%), 29 (32.3%), 33 (40.7%), 47 (43.8%), and 57 (41.2%). These extracts were found to lead to the successful synthesis of AgNPs when compared with the other extracts. The reducing power of each extract is shown in Figure 3. Extract number 3 had the highest reducing power with an absorbance of 0.91, and this value was set as 100% to compare the reducing power of the other extracts. Extract number 8 (95.6%) showed relatively high reducing power. The remaining four extracts possessed a medium range of reducing power among the fifty-eight extracts: 29 (30.8%), 33 (36.3%), 47 (51.7%), and 57 (40.7%).

3.3. Content of TPCs and reducing sugars of the fifty-eight extracts.

Together with the DPPH radical scavenging activity and reducing power, we proposed that the contents of TPCs and reducing sugars are also very influential for the synthesis of AgNPs. The TPC contents of the six extracts are shown in Figure 4. The highest TPC content was observed for extract number 47 (118.3 TPC content), and this value was set as 100%. The remaining extracts showed the following TPC contents when compared with extract number 47: 3 (90.5%), 8 (82.8%), 29 (80.9%), 33 (76.2%), and 57 (72.4%). All six extracts had relatively high TPC contents compared with the other extracts. Next, the reducing sugar content of the selected six extracts was also relatively high compared with the fifty-eight extracts (Figure 5). Extract number 8 showed the highest reducing sugar content, and this value was set as 100%. The reducing sugar contents of the remaining extracts were as follows: 3 (96.3%), 29 (37.8%), 33 (80.3%), 47 (66.3%), and 57 (70.4%). From these results, the high TPC and reducing sugar contents of the extracts were influential on the synthesis of AgNPs in the current report. It has been reported that plant extracts with high DPPH radical scavenging activity and high reducing power possess high content of phenolic compounds and reducing sugars [28,29]. Diverse primary and secondary metabolites including flavonoids, tannins, glucosides,

saponins and alkaloids were found at six selected plant extracts; *Areca catechu*, *Hypotrachyna laevigata*, *Ardisia incarnata*, *Maesa calophylla*, *Maesa laxiflora* and *Adinandra poilanei* [30-33]. These metabolites are most likely to contribute to the synthesis of AgNPs, thus it is one of our future works to investigate the phytochemical screening of six selected plant extracts.

3.4. FE-TEM images and size histograms of the six selected AgNP samples

The shapes and sizes of the six selected AgNP samples were observed by FE-TEM (Figure 6). All six AgNP samples were spherically shaped. Using the ImageJ program, the average size of each AgNP sample was measured from discrete nanoparticles in each image. The size histograms are displayed in Figure 7. The number of selected discrete nanoparticles to obtain each average size was as follows: (A) AgNPs-3 (100, 16.7 ± 0.2 nm), (B) AgNPs-8 (100, 21.3 ± 4.9 nm), (C) AgNPs-29 (100, 14.3 ± 0.2 nm), (D) AgNPs-33 (100, 14.5 ± 0.8 nm), (E) AgNPs-47 (100, 12.5 ± 1.0 nm), and (F) AgNPs-57 (100, 14.8 ± 0.6 nm). The smallest size was 12.5 ± 1.0 nm for AgNPs-47, and the largest size was 21.3 ± 4.9 nm for AgNPs-8. Except for AgNP-8 and AgNP-47, the remaining four AgNP samples showed a Gaussian distribution in their size histograms.

3.5. Shelf stability of the six selected AgNP samples

Colloidal stability of nanoparticle solutions is critical for *in vitro* and *in vivo* applications. The colloidal stability on the shelf for 28 days was assessed by acquiring UV-visible spectra for the six selected AgNP samples (Figure 8 and Table 3). The shape of the UV-visible spectra was fairly well retained for 28 days except for AgNPs-47 (Figure 8E). An absorbance decrease was observed for AgNPs-47 along with either a redshift or blueshift. The changes in the λ_{max} values observed over 28 days and are shown in Table 3. The value of λ_{max} was constant throughout 28 days for AgNPs-3,

AgNPs-8, AgNPs-29 and AgNPs-33. For AgNPs-47, a redshift was observed until day 21, and then a blueshift was observed at day 28. The major shift of AgNPs-57 was a blueshift. All shifts were in the range of less than 10 nm. Furthermore, no aggregation or agglomeration of the nanoparticle solutions were observed, suggesting that the colloidal stability was reasonably high after 28 days on the shelf in the dark. It is possible that the phytochemicals in each extract play a role in stabilizing the nanoparticles to retain colloidal stability on the shelf for 28 days.

3.6. Hydrodynamic sizes and zeta potentials of the six selected AgNP samples

The hydrodynamic sizes and zeta potential values were measured and are shown in Table 4. The hydrodynamic sizes were in the range of 49.5 ~ 122.6 nm with a polydispersity index of 0.137 ~ 0.230. Interestingly, all the zeta potentials were negative (-35.48 to -22.95 mV). The absolute value of each zeta potential was large enough to have excellent colloidal stability. This result corroborated well with the results the on the shelf colloidal stability from the previous section.

3.7. Cytotoxicity of the six selected AgNP samples

Cytotoxicity experiments of the six selected AgNP samples were performed in the A549 and HeLa cancer cell lines, and the results are shown in Figure 9. The cytotoxicity in each cell was very distinct for each AgNP sample. AgNPs-3 was very cytotoxic to A549 cells (viability of 56.4% to 54.6%) when compared with HeLa cells (viability of 93.1% to 92.7%). Interestingly, AgNPs-3 did not express any significant dose dependency on either cell line. The cytotoxicity of AgNPs-8 was similar in both cell lines at low (25 μM) and medium (50 μM) doses. At a high dose (100 μM), the cytotoxicity of AgNPs-8 increased in A549 cells (viability 50.6%), while the cytotoxicity did not change in HeLa cells (viability 90.7%). Most interestingly, both AgNPs-29 and AgNPs-33

demonstrated the highest cytotoxicity on A549 cells after treatment with a high dose (100 μM); AgNPs-29 (viability 10.9%) and AgNPs-33 (viability 8.1%). In HeLa cells, high cytotoxicity was also observed at the high dose of 100 μM for AgNPs-29 (viability 38.2%) and AgNPs-33 (viability 46.3%). Both AgNPs-29 and AgNPs-33 were more cytotoxic to A549 cells than HeLa cells the high dose (100 μM). A similar result was also observed for AgNPs-47, in which the viability was 25.6% for A549 cells and 66.0% for HeLa cells at the high dose of 100 μM.

When considering only the treatment at the high dose, the cytotoxicities were in the order of AgNPs-33 > AgNPs-29 > AgNPs-47 > AgNPs-8 > AgNPs-3 > AgNPs-57 in A549 cells. In HeLa cells, the order of cytotoxicities were AgNPs-29 > AgNPs-33 > AgNPs-47 > AgNPs-8 > AgNPs-3 > AgNPs-57. Specifically, at the high dose, three AgNP samples (AgNPs-29, AgNPs-33 and AgNPs-47) exerted relatively high cytotoxicity. Thus, we measured the cellular ROS generation, apoptosis/necrosis induction and cell cycle analysis in each cell line upon treatment with the six selected AgNP samples to explain the cytotoxicity results.

3.8. ROS generation of the six selected AgNP samples

AgNPs have been known to induce their cytotoxicity by ROS generation. The generation of ROS in A549 cells is presented in Figure 10. High ROS generation was clearly observed for AgNPs-29, AgNPs-33 and AgNPs-47, which also showed high cytotoxicity on A549 cells in the previous section. As demonstrated in Figure 10H, ROS generation in A549 cells was in the order of AgNPs-33 (49.50%) > AgNPs-29 (37.95%) > AgNPs-47 (22.22%) > AgNPs-8 (9.87%) > AgNPs-57 (6.90%) > AgNPs-3 (5.67%). Under the same conditions, ROS generation in the control was 4.26%. Three AgNP samples (AgNPs-33, AgNPs-29 and AgNPs-47) exhibited a remarkable increase in ROS generation: an 11.6-fold increase (AgNPs-33), an 8.9-fold increase (AgNPs-29), and a 5.2-fold increase (AgNPs-47) compared with the control.

In HeLa cells, a similar result was observed: the order of ROS generation was -29 (44.01%) > AgNPs-33 (30.06%) > AgNPs-47 (18.45%) > AgNPs-57 (5.47%) > AgNPs-8 (4.75%) > AgNPs-3 (4.67%). The fold increase of three AgNP samples was 12.4-fold (AgNPs-29), 8.5-fold (AgNPs-33) and 5.2-fold (AgNPs-47) when compared with the control. Observation of the increase in ROS generation demonstrated that the six selected AgNP samples in the current report induce ROS generation, resulting in oxidative stress and cell death. The cytotoxicity results in the previous section can be explained by the increase in ROS generation. The high cytotoxicity results from AgNPs-33, AgNPs-29 and AgNPs-47 correlated with the high generation of ROS.

When considering size and shape, all six AgNP samples had the same shape, and the average size was in the range of 12.5 ± 1.0 nm to 21.3 ± 4.9 nm. Thus, the size and shape of the nanoparticles did not significantly affect ROS generation. The zeta potentials were all negative; thus, surface charge was not a major factor affecting cytotoxicity and ROS generation. The discrepancy in cytotoxicity and ROS generation among the six selected AgNP samples is most likely due to the existence of various phytochemicals in each extract. It has been reported that antioxidants can protect against oxidative stress production during the course of disease, especially in cancer [34]. Polyphenols, which are major antioxidants, have been extensively investigated for their ability to reduce tumor growth *via* different mechanisms. Therefore, the phytochemicals (specifically polyphenols) that were bound to the surface of each AgNP sample can enable the regulation of internal ROS generation [34]. In fact, the content of TPCs differed among the fifty-eight extracts (Figure 4).

It is well recognized that treatments targeting ROS can be a new strategy for cancer therapy [35]. Anticancer drugs such as doxorubicin increase ROS generation in lung cancer and exert their anticancer activity by inhibition of serine/threonine-specific protein kinase [35]. Paclitaxel is an effective anticancer drug in lung and breast cancer by an ROS-dependent activation of apoptotic cell death [35]. ROS generation is also a pivotal reason of anticancer activity of AgNPs [36]. ROS-

mediated cytotoxicity in cancer affects signaling pathways and induces programmed cell death and cell cycle arrest [37].

3.9. Induction of apoptosis/necrosis of the six selected AgNP samples

In the previous section, ROS generation was closely related to cytotoxicity; thus, we performed Annexin V/PI staining to confirm apoptosis/necrosis. It is known that an increase in ROS generation can lead to apoptotic and necrotic cell death [38]. As shown in Figure 12 and Figure 13, early apoptosis was not observed. Moreover, cell death was mostly due to necrosis but very slightly due to late apoptosis in both A549 and HeLa cells. When comparing the two cell lines, the percentage of necrosis in A549 cells (Figure 12H) was higher than that in HeLa cells (Figure 13H) from the six selected AgNP samples. This result corroborated well with the cytotoxicity results in the previous section. In A549 cells, AgNPs-33 showed the highest necrosis percent (37.13%), followed by AgNPs-29 (29.69%) and AgNPs-8 (29.55%). AgNPs-8 had the highest late apoptosis percent of 11.85%. In HeLa cells, both AgNPs-29 (28.05%) and AgNPs-8 (23.03%) exhibited a high necrosis percent. The highest percent of late apoptosis in HeLa cells was observed from AgNPs-3 (3.37%).

Factors affecting the cellular fate from the nanoparticles were the shape, size, solubility, surface charge, crystallinity, ligand specificity and surface chemistry [38]. Additionally, the concentration (dose) can control different cellular fates, such as necrosis, apoptosis and autophagy. Specifically, the concentration is important for cell death induction by AgNPs. At low concentrations, necrosis and apoptosis generally occur, while necrosis alone is induced at high concentrations [38]. In the current report, we observed mostly necrosis with slight late apoptosis in A549 and HeLa cells. If the concentration of the AgNPs were to be changed, we could possibly observe different cell fates. Diverse phytochemicals in each extract lead to different surface chemistries of the AgNPs, which also affects cell death. Additionally, exposure time and tissue type affect cell fate. ROS generation by

nanoparticle exposure can result in (i) lipid peroxidation, (ii) protein denaturation and (iii) oxidative DNA damage [38]. It has been reported that increased ROS generation reduces the mitochondrial membrane potential and leads to mitochondrial membrane damage, which finally causes necrotic cell death [38].

3.10. Cell cycle analysis

The effects of the six selected AgNP samples were investigated by cell cycle analysis in A549 cells (Figure 14). An obvious increase in the cell population in the S phase was observed on AgNPs-29 (91.30%), AgNPs-33 (94.01%) and AgNPs-47 (78.36%) compared with the control (16.04%). AgNPs-3 (20.20%), AgNPs-8 (24.31%) and AgNPs-57 (23.76%) also showed slight increases in the S phase population. As shown in Figure 15, cell cycle analysis was performed in HeLa cells. Similar to the results from A549 cells, there was a significant increase in the S phase compared with the control (42.89%) as follows: AgNPs-29 (63.60%), AgNPs-33 (52.33%) and AgNPs-47 (50.83%). Furthermore, these three AgNP samples also showed an increased population of G2/M phase compared with the control (8.79%): AgNPs-29 (26.66%), AgNPs-33 (15.88%) and AgNPs-47 (17.83%). The other AgNP samples exhibited an increase in the G0/G1 phase compared with the control (43.01%): AgNPs-3 (59.22%), AgNPs-8 (63.71%) and AgNPs-57 (54.52%). According to our results, cell cycle arrest was dependent on the cell types that were used.

4. Conclusion

Plant extracts for the green synthesis of AgNPs are very beneficial, owing to their facile synthesis, environmentally friendly route and simple one-step process [39]. There are many reports regarding the green synthesis of AgNPs using plant extract, however, several plant extracts were utilized in

each report [40]. There is an important discrepancy between the current report and the other related articles. In the current report, fifty-eight plant extracts from Vietnam and Indonesia were screened under the same synthetic conditions in order to answer the following question; how factors (i.e. DPPH radical scavenging activity, reducing power, TPC contents and reducing sugar contents) affected the synthesis of AgNPs. Among the fifty-eight extracts, six extracts showed relatively high DPPH radical scavenging activity, high reducing power, high TPC contents and high reducing sugar contents. These extracts produced their corresponding AgNP samples successfully, and the six selected AgNP samples were synthesized with high yields. The six selected AgNP samples were all spherical shaped and had excellent stability on the shelf for 28 days. Specifically, diverse metabolites on the surface of AgNPs contributed to excellent stability along with biological activity.

The six selected AgNP samples showed relatively high cytotoxicity and excess ROS generation in cancer cell lines. The necrotic cell death of the six selected AgNP samples in the current report is largely related to increased intracellular ROS generation and subsequent substantial increase in cells in the S phase, which leads to cell cycle arrest of A549 and HeLa cells. Moreover, AgNPs green-synthesized by plant extracts generally have high antioxidant capability and anticancer activity, which leads to their possible therapeutic ability in cancer, and utilization of plant extracts as an important resource for the synthesis of AgNPs. Phytochemicals on the surface of AgNPs are most likely to be advantageous to cancer therapy; thus, green-synthesized AgNPs may be used for the treatment of cancer in the near future.

Funding: This work was supported by the National Research Foundation of Korea (NRF) through grants funded by the Korean government by the Ministry of Education (NRF-2015R1D1A1A09059054 and NRF-2018R1D1A1B07041709).

Acknowledgments: We acknowledge the receipt of material originating from Vietnam from the Joint Research Collaboration on Bioprospecting on Biological Materials of Vietnam between Institute of Ecology and Biological Resources, Socialist Republic of Vietnam (IEBR) and The Korea Research Institute of Bioscience and Biotechnology, Republic of Korea (KRIBB). We also acknowledge the receipt of material originating from Indonesia from the Joint Research Collaboration on Bioprospecting of Indonesian Plants between The Agency for the Assessment and Application of Technology, Republic of Indonesia (BPPT) and The Korea Research Institute of Bioscience and Biotechnology, Republic of Korea (KRIBB). The authors thank Ms. Hyesun Hong and Ms. Hye Eun Jeong for optimizing the synthetic conditions of the AgNPs.

References

[1] C. Damyanov, I. Maslev, V. Pavlov, L. Avramov, Conventional treatment of cancer realities and problems, Ann. Complement Altern. Med. 1 (2018) 1002.

[2] C. Liang, L. Xu, G. Song, Z. Liu, Emerging nanomedicine approaches fighting tumor metastasis: animal models, metastasis-targeted drug delivery, phototherapy, and immunotherapy, Chem. Soc. Rev. 45 (2016) 6250-6269.

[3] Y. Wang, S. Sun, Z. Zhang, D. Shi, Nanomaterials for cancer precision medicine, Adv. Mater. 30 (2018) e1705660.

[4] K.C. Hembram, R. Kumar, L. Kandha, P.K. Parhi, C.N. Kundu, B.K. Bindhani, Therapeutic prospective of plant-induced silver nanoparticles: application as antimicrobial and anticancer agent, Artif. Cells Nanomed. Biotechnol. 46 (2018) S38-S51.

[5] A.K. Mittal, Y. Chisti, U.C. Banerjee, Synthesis of metallic nanoparticles using plant extracts, Biotechnol. Adv. 31 (2013) 346-356.

[6] S. Jain, M.S. Mehata, Medicinal plant leaf extract and pure flavonoid mediated green synthesis of silver nanoparticles and their enhanced antibacterial property, Sci. Rep. 7 (2017) 1-13.

[7] M. Yadi, E. Mostafavi, B. Saleh, S. Davaran, I. Aliyeva, R. Khalilov, M. Nikzamir, N. Nikzamir, A. Akbarzadeh, Y. Panahi, Current developments in green synthesis of metallic nanoparticles using plant extracts: a review, Artif. Cells Nanomed. Biotechnol. 46 (2018) S336-S343.

[8] M. Ovais, A.T. Khalil, A. Raza, M.A. Khan, I. Ahmad, N.U. Islam, M. Saravanan, M.F. Ubaid, M. Ali, Z.K. Shinwari, Green synthesis of silver nanoparticles via plant extracts: beginning a new era in cancer theranostics. Nanomedicine, 12 (2016) 3157-3177.

[9] Y. Park, New paradigm shift for the green synthesis of antibacterial silver nanoparticles utilizing plant extracts, Toxicol. Res. 30 (2014) 169-178.

[10] Y. Park, Y. Hong, A. Weyers, Y. Kim, R. Linhardt, Polysaccharides and phytochemicals: a natural reservoir for the green synthesis of gold and silver nanoparticles, IET Nanobiotechnol. 5 (2011) 69-78

[11] A.K. Shukla, S. Iravani, Green synthesis, characterization and applications of nanoparticles, Elsevier, 2018.

[12] E.-Y. Ahn, H. Jin, Y. Park, Assessing the antioxidant, cytotoxic, apoptotic and wound healing properties of silver nanoparticles green-synthesized by plant extracts, Mater. Sci. Eng. C Mater. Biol. Appl. 101 (2019) 204-216.

[13] R. Subramanian, P. Subbramaniyan, V. Raj, Antioxidant activity of the stem bark of *Shorea roxburghii* and its silver reducing power, SpringerPlus 2 (2013) 28.

[14] N.S. Jalani, S. Zati-Hanani, Y.P. Teoh, R. Abdullah, in: Short review: the effect of reaction conditions on plant-mediated synthesis of silver nanoparticles, Materials Science Forum, Trans. Tech. Publ. 2018, pp. 145-151.

[15] H.S. Kim, Y.S. Seo, K. Kim, J.W. Han, Y. Park, S. Cho, Concentration effect of reducing agents on green synthesis of gold nanoparticles: size, morphology, and growth mechanism, Nanoscale Res. Lett. 11 (2016) 230.

[16] N.A. Hanan, H.I. Chiu, M.R. Ramachandran, W.H. Tung, M. Zain, N. Nadhirah, N. Yahaya, V. Lim, Cytotoxicity of plant-mediated synthesis of metallic nanoparticles, a systematic review. Int. J. Mol. Sci. 19 (2018) 1725.

[17] H. Barabadi, M. Ovais, Z.K. Shinwari, M. Saravanan, Anti-cancer green bionanomaterials: present status and future prospects, Green Chem. Lett. Rev. 10 (2017) 285-314.

[18] F. Ahmad, N. Ashraf, T. Ashraf, R.-B. Zhou, D.-C. Yin, Biological synthesis of metallic nanoparticles (MNPs) by plants and microbes: their cellular uptake, biocompatibility, and biomedical applications, Appl. Microbiol. Biotechnol. 103 (2019) 2913-2935.

[19] C. Carnovale, G. Bryant, R. Shukla, V. Bansal, Size, shape and surface chemistry of nano-gold dictate its cellular interactions, uptake and toxicity, Prog. Mater. Sci. 83 (2016) 152-190.

[20] P.V. Rao, D. Nallappan, K. Madhavi, S. Rahman, L. Jun Wei, S.H. Gan, Phytochemicals and biogenic metallic nanoparticles as anticancer agents. Oxi. Med. Cell Longev. 2016 (2016) 3685671.

[21] L.Z. Flores-López, H. Espinoza-Gómez, R. Somanathan, Silver nanoparticles: electron transfer, reactive oxygen species, oxidative stress, beneficial and toxicological effects. mini review. J. Appl. Toxicol. 39 (2019) 16-26.

[22] S. Chanda, R. Dave, *In vitro* models for antioxidant activity evaluation and some medicinal plants possessing antioxidant properties: An overview. Afr. J. Microbiol. Res. 3 (2009) 981-996.

[23] A.V. Gusakov, E.G. Kondratyeva, A.P. Sinitsyn, Comparison of two methods for assaying reducing sugars in the determination of carbohydrase activities, Int. J. Anal. Chem. 2011 (2011) 283658.

[24] E.-Y. Ahn, H. Jin, Y. Park, Green synthesis and biological activities of silver nanoparticles prepared by *Carpesium cernuum* extract, Arch. Pharm. Res. 42 (2019) 926-934.

[25] Y.J. Lee, E.-Y. Ahn, Y. Park, Shape-dependent cytotoxicity and cellular uptake of gold nanoparticles synthesized using green tea extract. Nanoscale Res. Lett. 14 (2019) 129.

[26] V. De Matteis, M. Cascione, C.C. Toma, S. Leporatti, Silver nanoparticles: synthetic routes, in vitro toxicity and theranostic applications for cancer disease, Nanomaterials 8 (2018) 319.

[27] A.A. Zahir, I.S. Chauhan, A. Bagavan, C. Kamaraj, G. Elango, J. Shankar, N. Arjaria, S.M. Roopan, A.A. Rahuman, N. Singh, Green synthesis of silver and titanium dioxide nanoparticles using Euphorbia prostrata extract shows shift from apoptosis to G0/G1 arrest followed by necrotic cell death in Leishmania donovani, Antimicrob. Agents Chemother. 59 (2015) 4782-4799.

[28] S. Dudonné, X. Vitrac, P. Coutière, M. Woillez, J.-M. Mérillon, Comparative study of antioxidant properties and total phenolic content of 30 plant extracts of industrial interest using DPPH, ABTS, FRAP, SOD, and ORAC assays, J. Agric. Food Chem. 57 (2009) 1768-1774.

[29] N. Paixão, R. Perestrelo, J.C. Marques, J.S. Câmara, Relationship between antioxidant capacity and total phenolic content of red, rose and white wines, Food Chem. 105 (2007) 204-214.

[30] M.Senthil Amudhan, V. Hazeena Begum, K.B. Hebbar, A review on phytochemical and pharmacological potential of *Areca catechu* L. seed, Int. J. Pharm. Sci. Res. 3 (2012) 4151-4157.

[31] J.R.L. Walker, E.A. Lintott, A phytochemical register of New Zealand lichens, New Zealand Journal of Botany, 35 (1997) 369-384.

[32] N.T.H. Van, C. Rivière, P.Q. Long, T.A. Vien, P.V. Kiem, C.V. Minh, Flavonoids, megastigmanes and other constituents from *Ardisia incarnata*, Biochem. Syst. Ecol. 61 (2015) 413-416.

[33] Z. Jiang, J.F. Gallard, M.T. Adeline, V. Dumontet, M.V. Tri, T. Sévenet, M. Païs, Six triterpenoid saponins from *Maesa laxiflora*, J. Nat. Prod. 62 (1999) 873-876.

[34] M.A. Ebrahimzadeh, A. Tafazoli, J. Akhtari, P. Biparva, S. Eslami, Engineered silver nanoparticles, a new nanoweapon against cancer, Anti-Cancer Agents Med. Chem. 18 (2018) 1962-1969.

[35] S. Mitra, L.N. Nguyen, M. Akter, G. Park, E.H. Choi, N.K. Kaushik, Impact of ROS generated by chemical, physical, and plasma techniques on cancer attenuation. Cancers, 11 (2019) 1030-1061.

[36] M. Ovais, A.T. Khalil, A. Raza. M.A. Khan, I. Ahmad, N.U. Islam, M. Saravanan, M.F. Ubaid, M. Ali, Z.K. Shinwari, Green synthesis of silver nanoparticles via plant extracts: Beginning a new era in cancer theranostics. Nanomedicine 12 (2016) 3157-3177.

[37] S. NavaneethaKrishnan, J.L. Rosales, K.Y. Lee, ROS-mediated cancer cell killing through dietary phytochemicals. Oxid Med Cell Longev. 2019 (2019) 9051542.

[38] R. Mohammadinejad, M.A. Moosavi, S. Tavakol, D.Ö. Vardar, A. Hosseini, M. Rahmati, L. Dini, S. Hussain, A. Mandegary, D.J. Klionsky, Necrotic, apoptotic and autophagic cell fates triggered by nanoparticles, Autophagy, 15 (2019) 4-33.

[39] L.P. Silva, T.M. Pereira, C.C. Bonatto, Frontiers and perspectives in the green synthesis of silver nanoparticles, in: Green Synthesis, Characterization and Applications of Nanoparticles, Elsevier, 2019, pp. 137-164.

[40] M. Das, S. Chatterjee, Green synthesis of metal/metal oxide nanoparticles toward biomedical applications: boon or ban, in: Green synthesis, characterization and applications of nanoparticles, Elsevier, 2019, pp. 265-301.

Table 1. Fifty-eight plant extracts from Vietnam and Indonesia were used in the current report.

No.	scientific name	genus	parts used for extraction	extraction solvent[a]	origin
1	*Bridelia monoica*	Euphorbiaceae	leaves, twigs	methanol	Vietnam
2	*Broussonetia papyrifera*	Moraceae	leaves, twig	methanol	Vietnam
3	*Areca catechu*	Arecaceae	fruits	ethanol	Indonesia
4	*Baeckea frutescens*	Myrtaceae	leaves	ethanol	Indonesia
5	*Curcuma aromatica*	Zingiberaceae	roots	ethanol	Indonesia
6	*Curcuma longa*	Zingiberaceae	roots	ethanol	Indonesia
7	*Elaeocarpus grandiflorus*	Elaeocarpaceae	fruits	ethanol	Indonesia
8	*Hypotrachyna laevigata*	Parmeliaceae	barks	ethanol	Indonesia
9	*Kaempferia pandurata*	Zingiberaceae	roots	ethanol	Indonesia
10	*Ardisia pseudocrispa*	Primulaceae	leaves, twigs	methanol	Vietnam
11	*Ardisia pseudo-pedunculosa*	Primulaceae	leaves, twigs	methanol	Vietnam
12	*Glycosmis ovoidea*	Rutaceae	leaves, twigs	methanol	Vietnam
13	*Combretum quadrangulare*	Combretaceae	leaves, twigs	methanol	Vietnam
14	*Sesbania javanica*	Fabaceae	leaves, twigs, flowers	methanol	Vietnam
15	*Polyalthia longifolia*	Annonaceae	leaves, twigs	methanol	Vietnam
16	*Gardenia annamensis*	Rubiaceae	leaves, twigs	methanol	Vietnam
17	*Archidendron kerrii*	Fabaceae	leaves, twigs	methanol	Vietnam
18	*Murraya koenigii*	Rutaceae	leaves, twigs, fruits	methanol	Vietnam
19	*Pittosporum merrillianum*	Pittosporaceae	leaves, twigs	methanol	Vietnam
20	*Agave americana*	Asparagaceae	whole plant	methanol	Vietnam
21	*Desmodium laxiflorum*	Fabaceae	leaves	methanol	Indonesia
22	*Catunaregam spinosa*	Rubiaceae	leaves	methanol	Indonesia
23	*Momordica charantia*	Cucurbitaceae	leaves	methanol	Indonesia
24	*Saccopetalum horsfieldii*	Annonaceae	leaves	methanol	Indonesia
25	*Aglaia odorata*	Meliaceae	leaves	methanol	Indonesia
26	*Casearia grewiifolia*	Salicaceae	leaves	methanol	Indonesia
27	*Mitrephora javanica*	Annonaceae	leaves	methanol	Indonesia
28	*Maesa indica*	Myrsinaceae	leaves, twigs, flowers	methanol	Vietnam
29	*Ardisia incarnata*	Myrsinaceae	leaves, twigs, fruits	methanol	Vietnam
30	*Chisocheton microcarpus*	Meliaceae	leaves	methanol	Indonesia
31	*Polyscias scutellaria*	Araliaceae	leaves, twigs	methanol	Vietnam
32	*Dodonaea angustifolia*	Sapindaceae	leaves, twigs, fruits	methanol	Vietnam
33	*Maesa calophylla*	Myrsinaceae	leaves, twigs, flowers	methanol	Vietnam
34	*Merremia vitifolia*	Convolvulaceae	leaves, twigs, flowers	methanol	Vietnam
35	*Beaumontia grandiflora*	Apocynaceae	leaves, twigs	methanol	Vietnam
36	*Borassus flabellifer*	Arecaceae	leaves, twigs	methanol	Vietnam
37	*Maesa subdentata*	Myrsinaceae	leaves, twigs	methanol	Vietnam
38	*Altingia takhtajanii*	Altingiaceae	leaves, twigs	methanol	Vietnam
39	*Ormosia sumatrana*	Fabaceae	leaves, twigs, flowers	methanol	Vietnam
40	*Maesa tenera*	Myrsinaceae	leaves, twigs	methanol	Vietnam
41	*Persea pierrei*	Lauraceae	leaves, twigs	methanol	Vietnam
42	*Ardisia macrophylla*	Myrsinaceae	leaves	methanol	Indonesia

43	*Solanum nigrum*	Solanaceae	leaves	methanol	Indonesia
44	*Labisia pumila*	Myrsinaceae	leaves	methanol	Indonesia
45	*Trevesia palmata*	Araliaceae	leaves, stems, flowers	methanol	Vietnam
46	*Polyscias guilfoylei*	Araliaceae	leaves, twigs	methanol	Vietnam
47	*Maesa laxiflora*	Myrsinaceae	leaves, twigs	methanol	Vietnam
48	*Pittosporum balansae*	Pittosporaceae	leaves, twigs	methanol	Vietnam
49	*Pittosporum kerrii*	Pittosporaceae	leaves, twigs	methanol	Vietnam
50	*Heterostemma grandiflorum*	Asclepiadaceae	leaves, twigs, flowers	methanol	Vietnam
51	*Sphagneticola trilobata*	Asteraceae	leaves	methanol	Indonesia
52	*Viburnum lutescens*	Caprifoliaceae	leaves	methanol	Indonesia
53	*Euphorbia cotinifolia*	Euphorbiaceae	leaves	methanol	Indonesia
54	*Corypha utan*	Arecaceae	leaves	methanol	Indonesia
55	*Schefflera rugosa*	Araliaceae	leaves	methanol	Indonesia
56	*Maesa membranacea*	Myrsinaceae	leaves, twigs	methanol	Vietnam
57	*Adinandra poilanei*	Pentaphylacaceae	leaves, twigs	methanol	Vietnam
58	*Ardisia virens*	Myrsinaceae	leaves, twigs, fruits	methanol	Vietnam

[a]methanol (99.9%), ethanol (aqueous, 95%)

Table 2. Synthetic yield (%) of the six selected AgNP samples.

samples	yield (%)
AgNPs-3	99.08
AgNPs-8	91.61
AgNPs-29	99.26
AgNPs-33	99.33
AgNPs-47	99.51
AgNPs-57	99.66

Table 3. Shelf stability on the six selected AgNP samples. Changes in λ_{max} (nm) values were observed for 28 days.

	day 0	**day 1**	**day 2**	**day 5**	**day 7**	**day 14**	**day 21**	**day 28**
AgNPs-3	416	416	416	416	416	416	416	416
AgNPs-8	428	428	428	428	428	428	428	428
AgNPs-29	432	432	432	432	432	432	432	432
AgNPs-33	434	434	434	434	434	434	434	434
AgNPs-47	430	438	438	438	438	440	436	428
AgNPs-57	438	430	430	430	430	430	430	433

Table 4. Hydrodynamic sizes and zeta potentials of the six selected AgNP samples.

samples	hydrodynamic size (nm)	polydispersity index	zeta potential (mV)
AgNPs-3	104.0	0.174	-26.08
AgNPs-8	49.5	0.137	-22.95
AgNPs-29	99.1	0.209	-27.99
AgNPs-33	122.6	0.190	-26.55
AgNPs-47	102.5	0.191	-35.48
AgNPs-57	111.7	0.230	-28.78

Figure legends

Figure 1. UV-visible spectra of AgNPs synthesized with the fifty-eight plant extracts. The six selected AgNP samples are colored yellow and were used for further study.

Figure 2. DPPH radical scavenging activity of the fifty-eight extracts.

Figure 3. Reducing power of the fifty-eight extracts.

Figure 4. Total phenolic compound content of the fifty-eight extracts.

Figure 5. Reducing sugars content of the fifty-eight extracts.

Figure 6. FE-TEM images of the six selected AgNP samples. (A) AgNPs-3, (B) AgNPs-8, (C) AgNPs-29, (D) AgNPs-33, (E) AgNPs-47, and (F) AgNPs-58. The scale bars represent 200 nm (left images) and 50 nm (right images).

Figure 7. Size histograms of the six selected AgNP samples. (A) AgNPs-3, (B) AgNPs-8, (C) AgNPs-29, (D) AgNPs-33, (E) AgNPs-47, and (F) AgNPs-58.

Figure 8. Shelf stability of the six selected AgNP samples. (A) AgNPs-3, (B) AgNPs-8, (C) AgNPs-29, (D) AgNPs-33, (E) AgNPs-47, and (F) AgNPs-58. Changes in the visible spectrum were observed for 28 days.

Figure 9. Cytotoxicities of the six selected AgNP samples in cancer cell lines. (A) A549 cells and (B) HeLa cells.

Figure 10. ROS generation in A549 cells upon treatment with the six selected AgNP samples. (A) Control, (B) AgNPs-3, (C) AgNPs-8, (D) AgNPs-29, (E) AgNPs-33, (F) AgNPs-47, (G) AgNPs-57, and (H) the percentages of cellular ROS generated by cells exposed to the six selected AgNPs for 24 h.

Figure 11. ROS generation in HeLa cells upon treatment with the six selected AgNP samples. (A) Control (B) AgNPs-3, (C) AgNPs-8, (D) AgNPs-29, (E) AgNPs-33, (F) AgNPs-47, (G) AgNPs-57,

and (H) the percentages of cellular ROS generated by cells exposed to the six selected AgNPs for 24 h.

Figure 12. Apoptosis assay of the six selected AgNP samples in A549 cells. (A) Control (B) AgNPs-3, (C) AgNPs-8, (D) AgNPs-29, (E) AgNPs-33, (F) AgNPs-47, (G) AgNPs-57, and (H) the percentages of four proportions of cells exposed to the selected six AgNPs for 24 h.

Figure 13. Apoptosis assay of the six selected AgNP samples in HeLa cells. (A) Control (B) AgNPs-3, (C) AgNPs-8, (D) AgNPs-29, (E) AgNPs-33, (F) AgNPs-47, (G) AgNPs-57, and (H) the percentages of four proportions of cells exposed to the selected six AgNPs for 24 h.

Figure 14. Cell cycle arrest in A549 cells upon treatment with the six selected AgNP samples. (A) Control (B) AgNPs-3, (C) AgNPs-8, (D) AgNPs-29, (E) AgNPs-33, (F) AgNPs-47, (G) AgNPs-57, and (H) the percentages of each cell cycle phase after exposure of the cells to the six selected AgNPs for 24 h.

Figure 15. Cell cycle arrest on HeLa cells upon treatment of the six selected AgNP samples (A) control (B) AgNP-3, (C) AgNP-8, (D) AgNP-29, (E) AgNP-33, (F) AgNP-47, (G) AgNP-57, and (H) the percentages of each cell cycle phase after exposure of the cells to the six selected AgNPs for 24 h.

Figure 1.

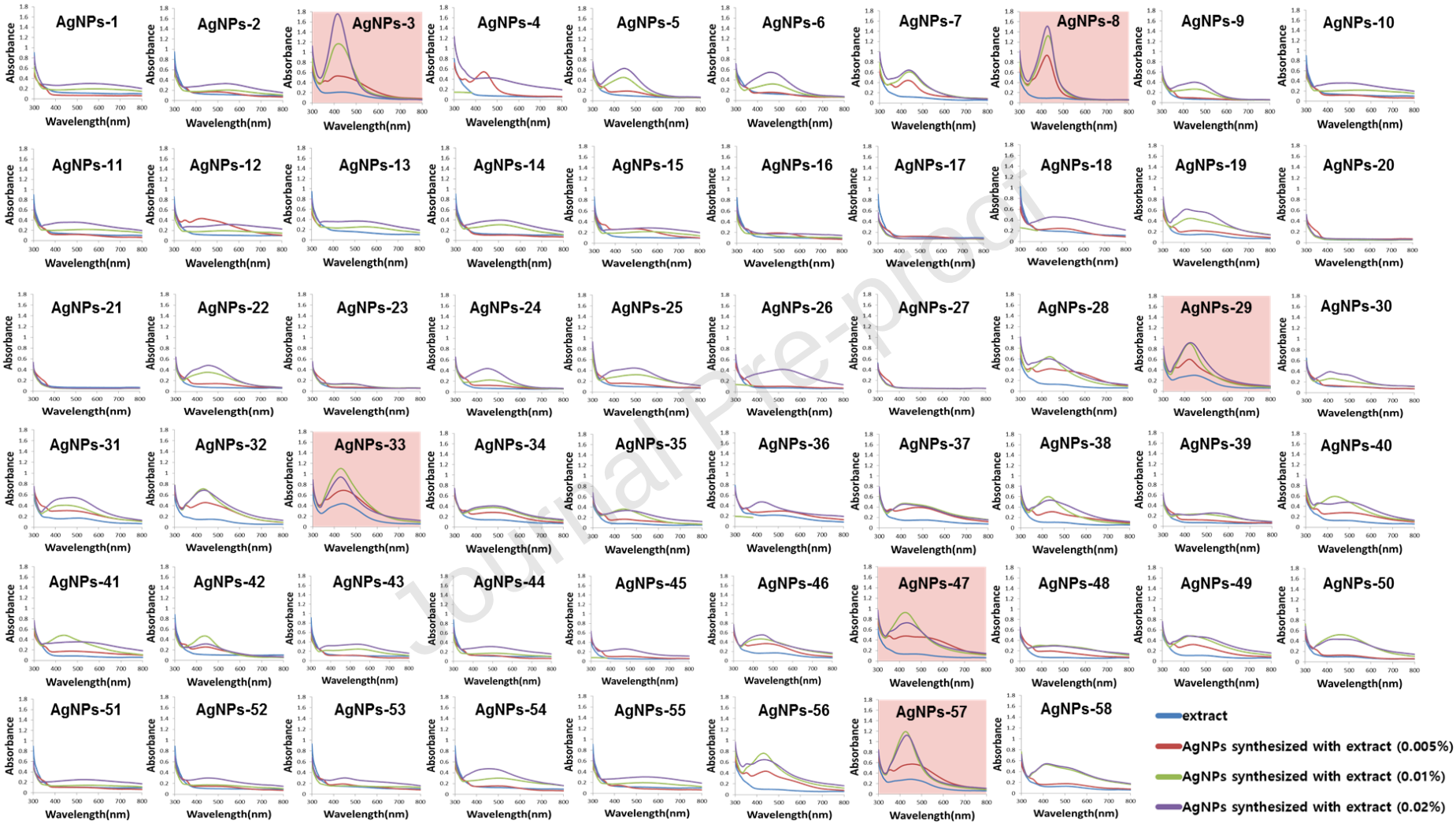
AgNPs-1
AgNPs-2
AgNPs-3
AgNPs-4
AgNPs-5
AgNPs-6
AgNPs-7
AgNPs-8
AgNPs-9
AgNPs-10
AgNPs-11
AgNPs-12
AgNPs-13
AgNPs-14
AgNPs-15
AgNPs-16
AgNPs-17
AgNPs-18
AgNPs-19
AgNPs-20
AgNPs-21
AgNPs-22
AgNPs-23
AgNPs-24
AgNPs-25
AgNPs-26
AgNPs-27
AgNPs-28
AgNPs-29
AgNPs-30
AgNPs-31
AgNPs-32
AgNPs-33
AgNPs-34
AgNPs-35
AgNPs-36
AgNPs-37
AgNPs-38
AgNPs-39
AgNPs-40
AgNPs-41
AgNPs-42
AgNPs-43
AgNPs-44
AgNPs-45
AgNPs-46
AgNPs-47
AgNPs-48
AgNPs-49
AgNPs-50
AgNPs-51
AgNPs-52
AgNPs-53
AgNPs-54
AgNPs-55
AgNPs-56
AgNPs-57
AgNPs-58
Absorbance
Wavelength(nm)
extract
AgNPs synthesized with extract (0.005%)
AgNPs synthesized with extract (0.01%)
AgNPs synthesized with extract (0.02%)

Figure 2.

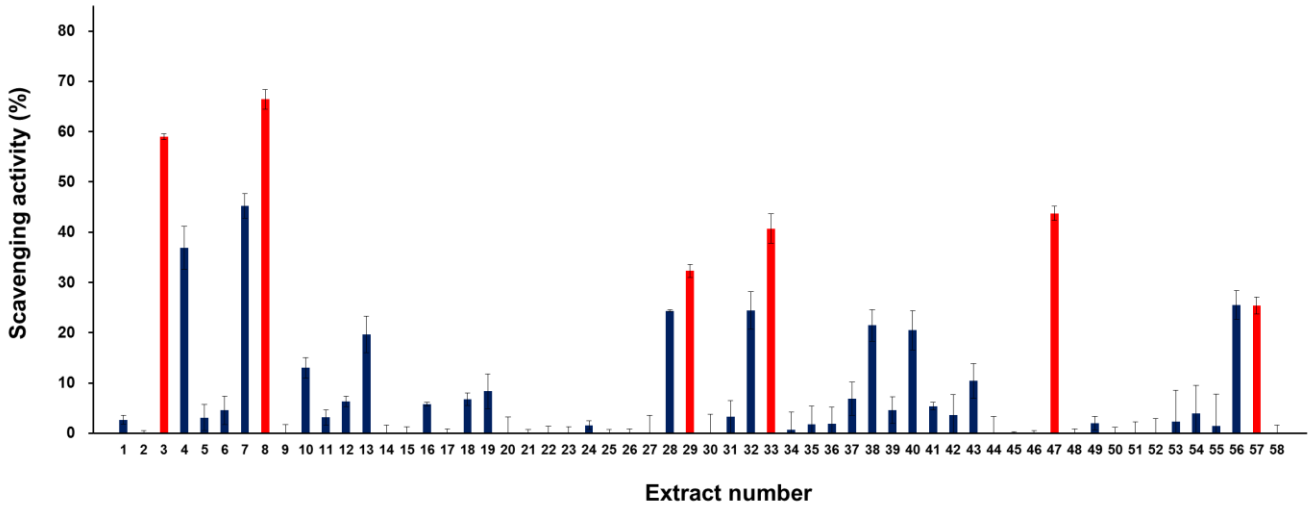

Figure 3.

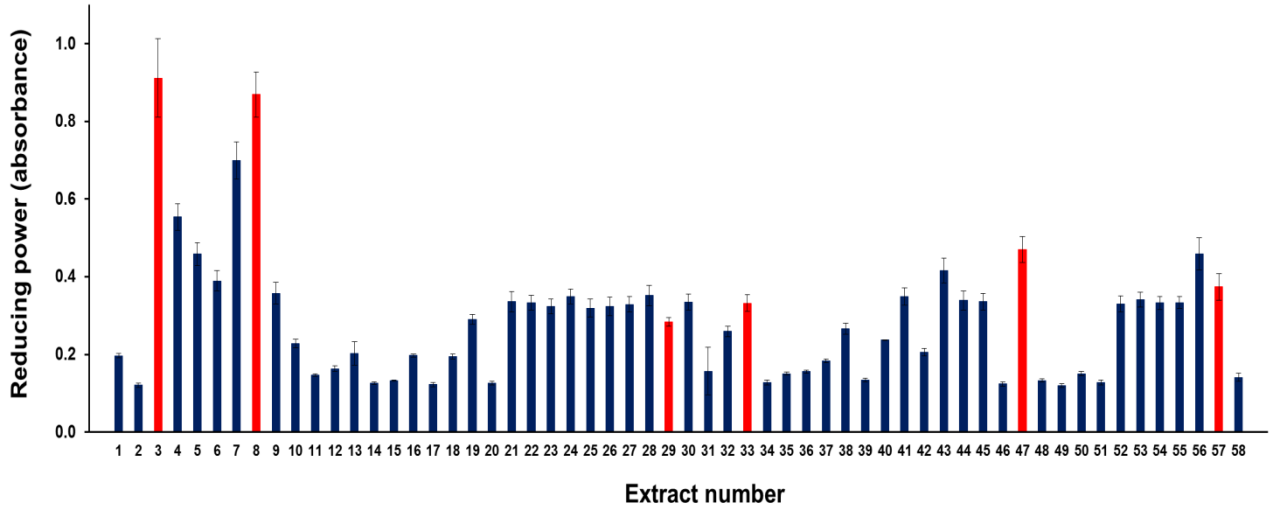

Figure 4.

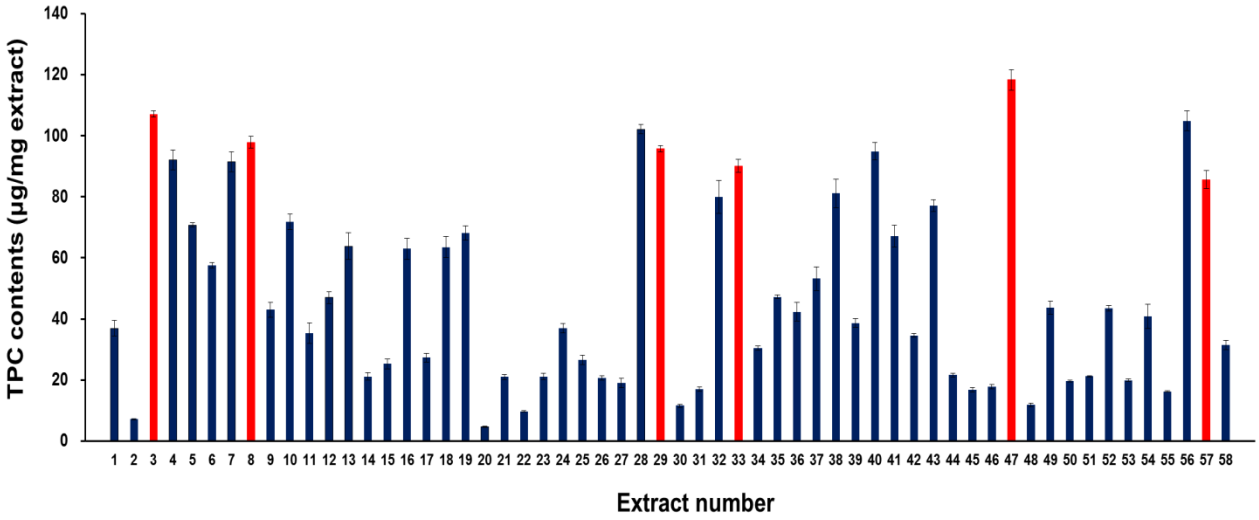

Figure 5.

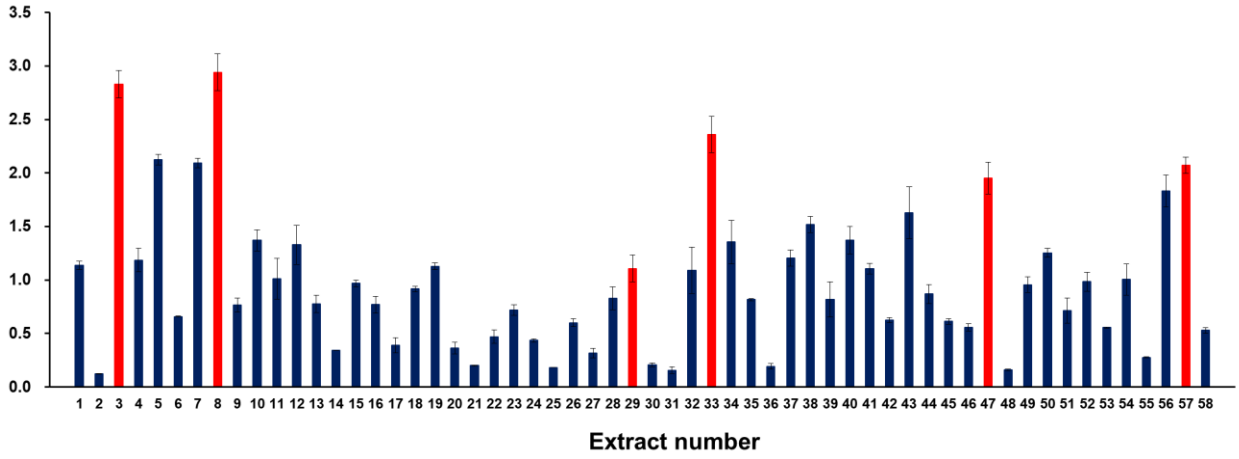

Figure 6.

(A)

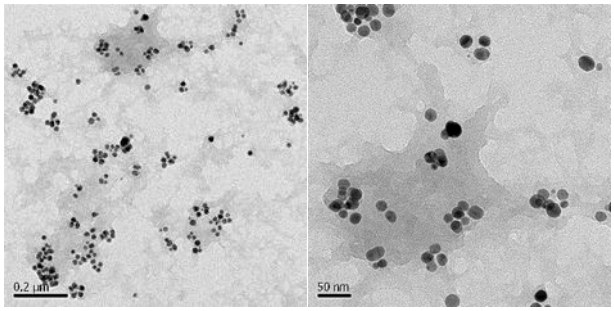

(B)

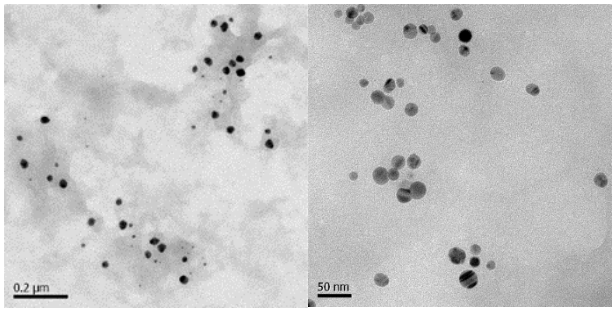

(C)

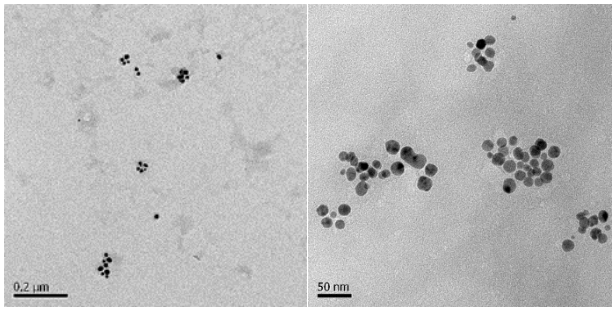

(D)

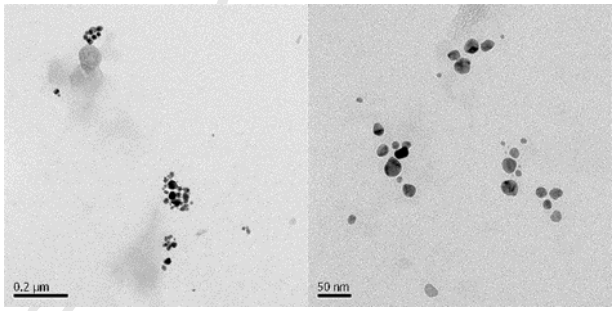

(E)

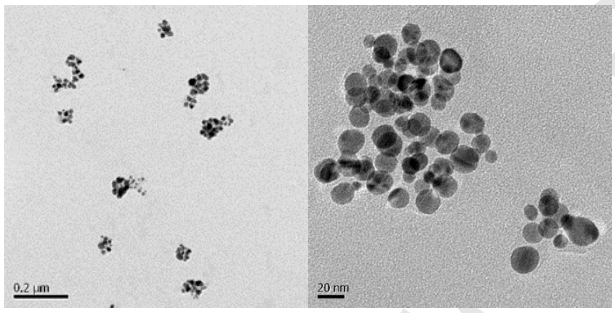

(F)

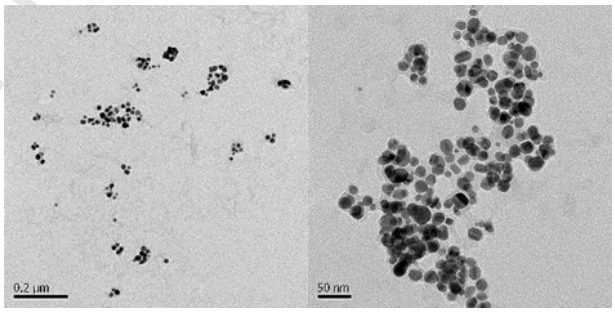

Figure 7.

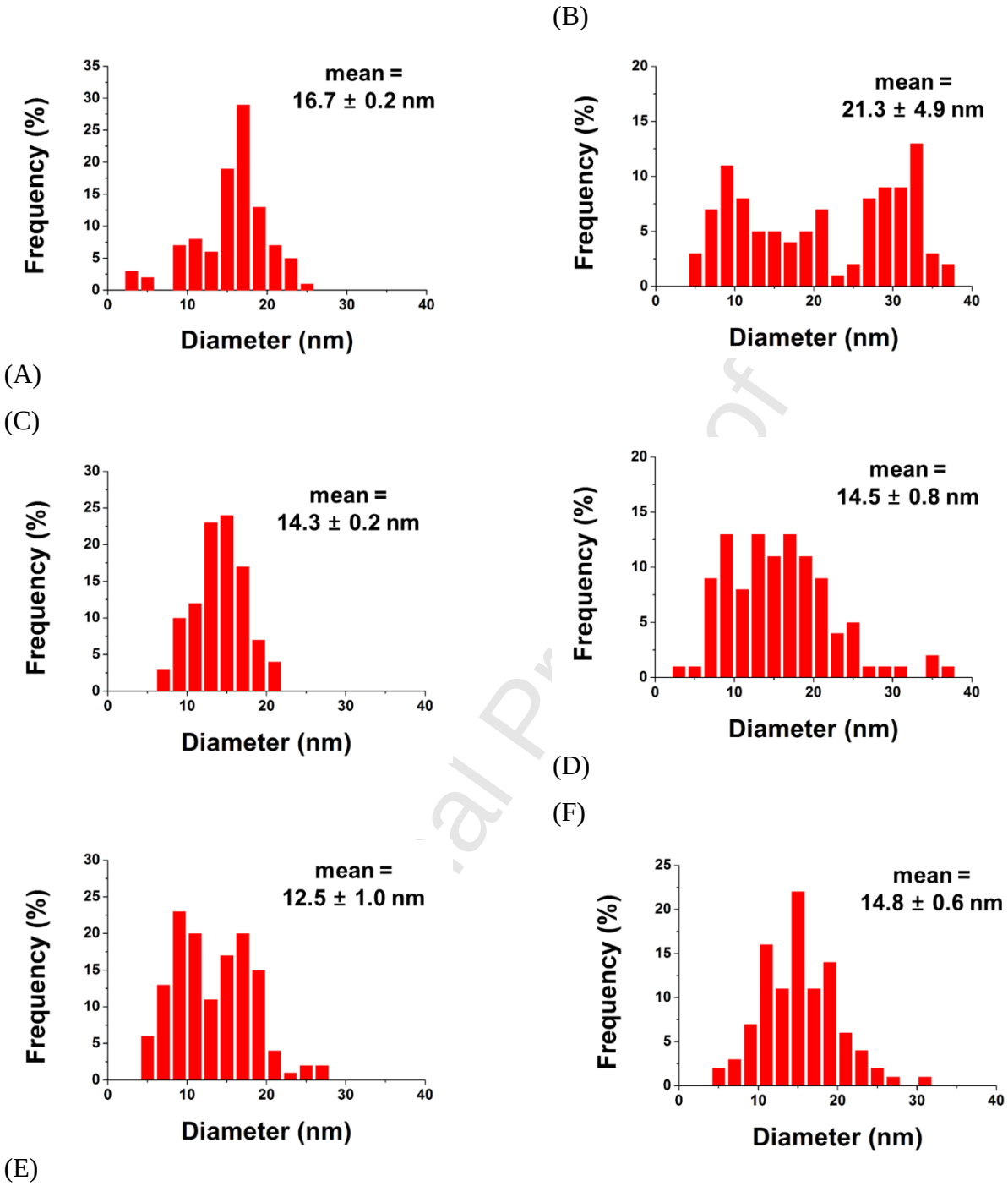
(A)
mean =
16.7 ± 0.2 nm
Frequency (%)
Diameter (nm)
(B)
mean =
21.3 ± 4.9 nm
Frequency (%)
Diameter (nm)
(C)
mean =
14.3 ± 0.2 nm
Frequency (%)
Diameter (nm)
(D)
mean =
14.5 ± 0.8 nm
Frequency (%)
Diameter (nm)
(E)
mean =
12.5 ± 1.0 nm
Frequency (%)
Diameter (nm)
(F)
mean =
14.8 ± 0.6 nm
Frequency (%)
Diameter (nm)

Figure 8.

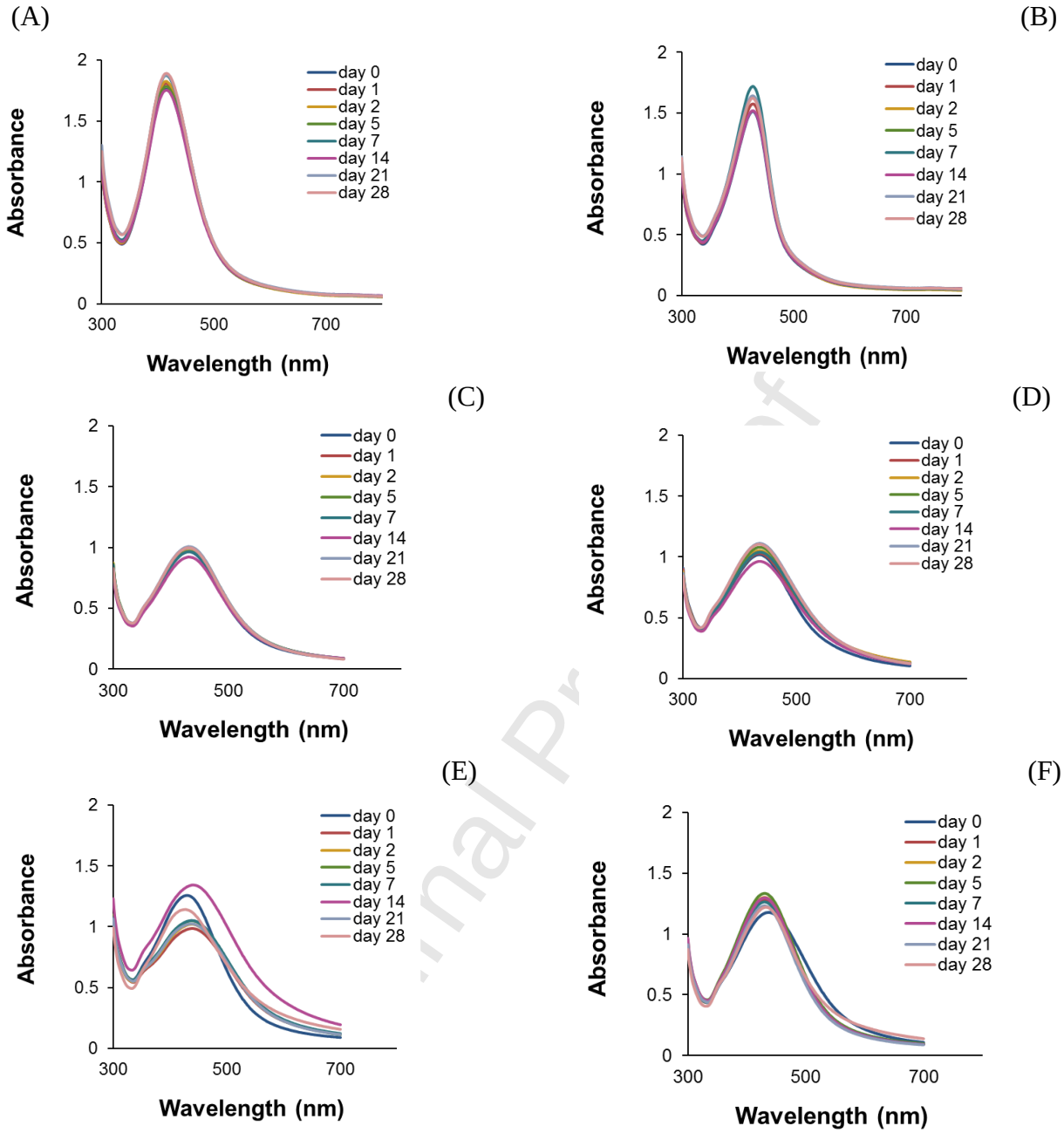
(A)
(B)
(C)
(D)
(E)
(F)
Absorbance
Wavelength (nm)
day 0
day 1
day 2
day 5
day 7
day 14
day 21
day 28

Figure 9.

(A)

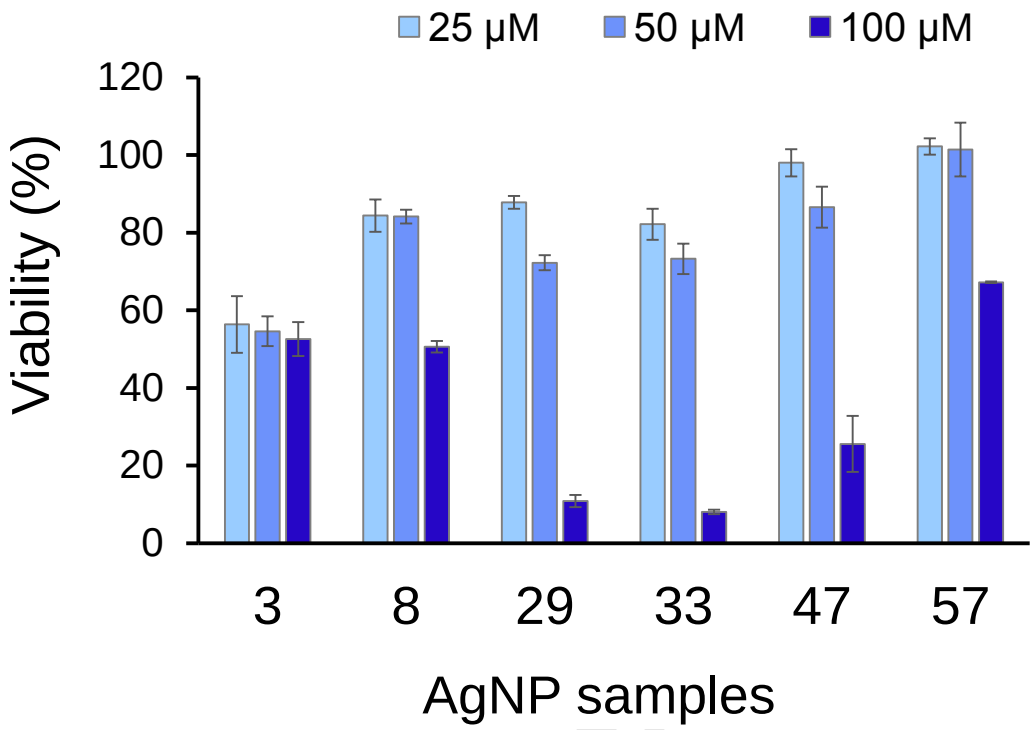
25 µM
50 µM
100 µM
Viability (%)
120
100
80
60
40
20
0
3
8
29
33
47
57
AgNP samples

(B)

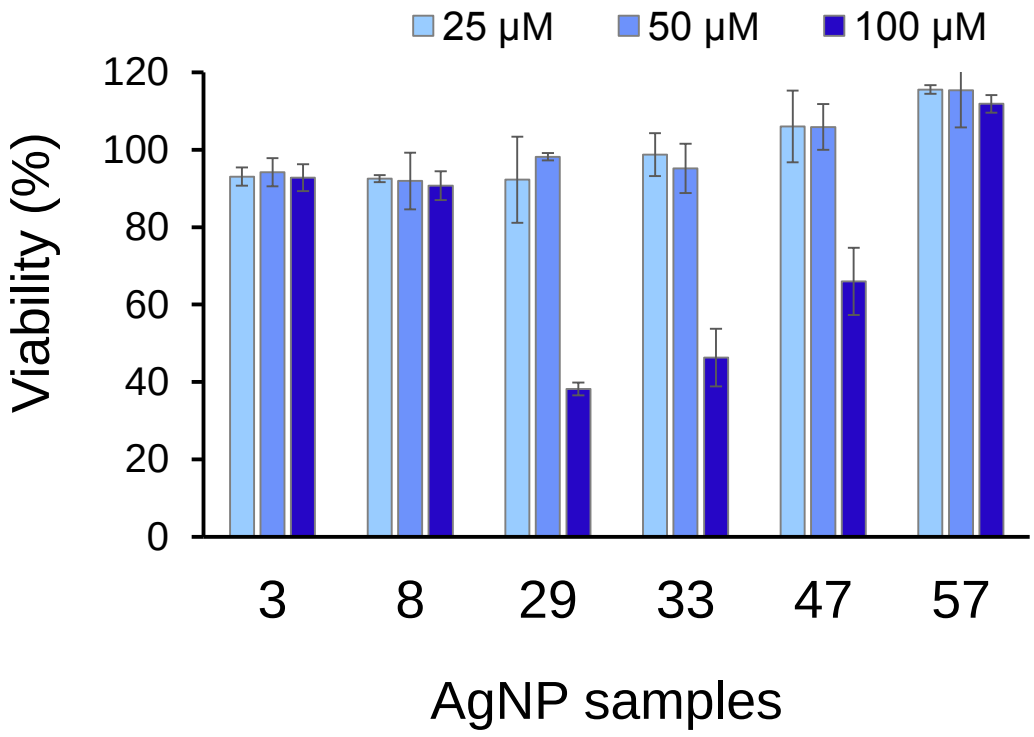
25 µM
50 µM
100 µM
Viability (%)
120
100
80
60
40
20
0
3
8
29
33
47
57
AgNP samples

Figure 10.

(A) control

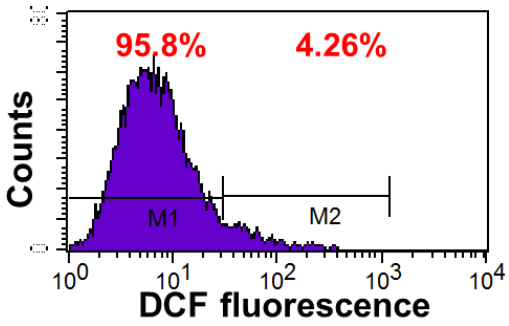

(B) AgNPs-3

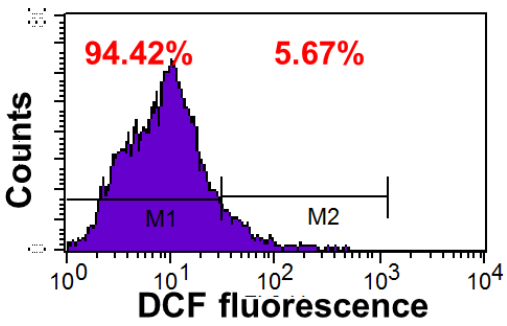

(C) AgNPs-8

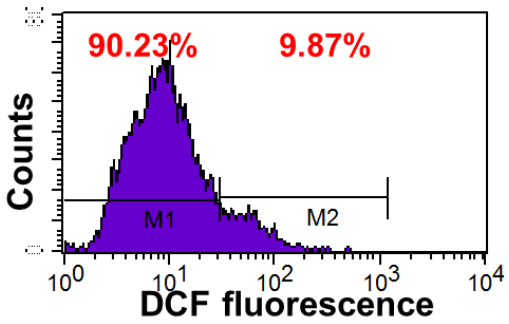

(D) AgNPs-29

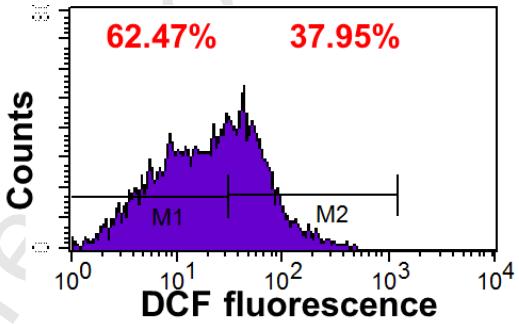

(E) AgNPs-33

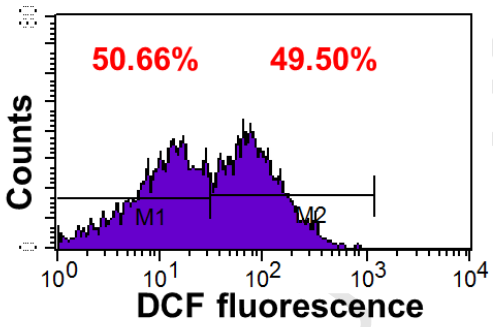

(F) AgNPs-47

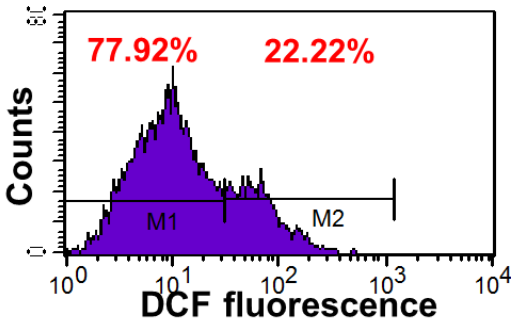

(G) AgNPs-57

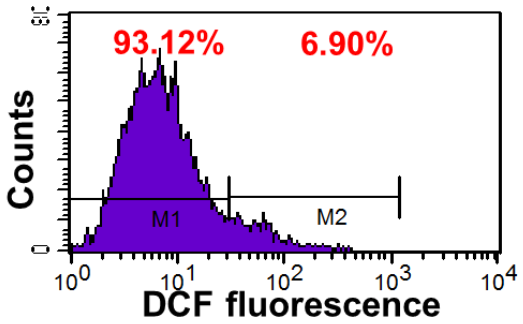

(H)

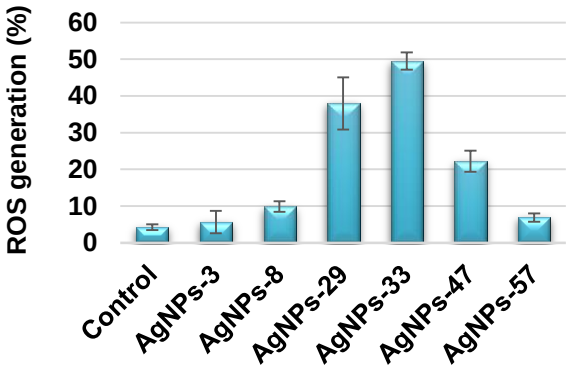

Figure 11.

(A) control

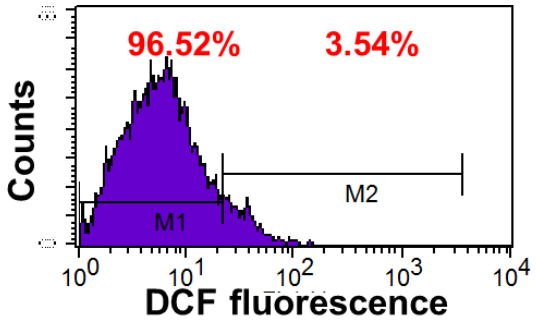

(B) AgNPs-3

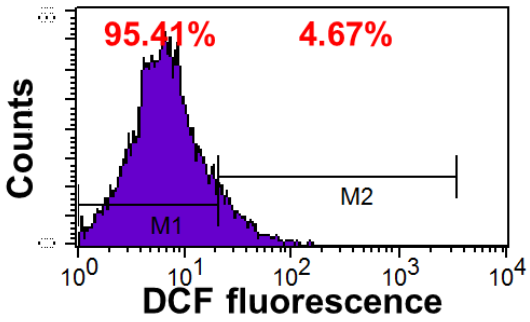

(C) AgNPs-8

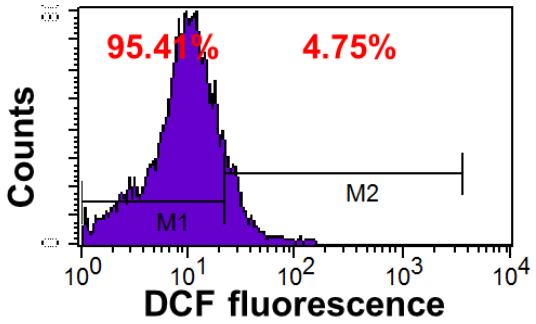

(D) AgNPs-29

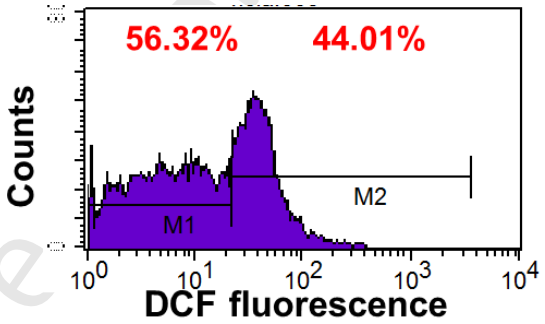

(E) AgNPs-33

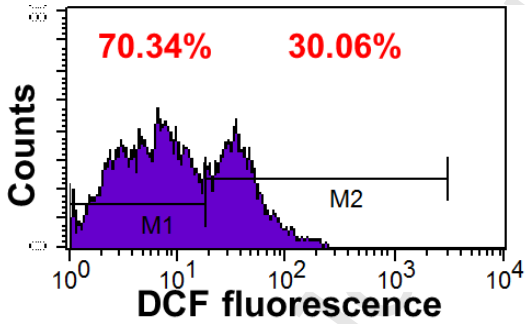

(F) AgNPs-47

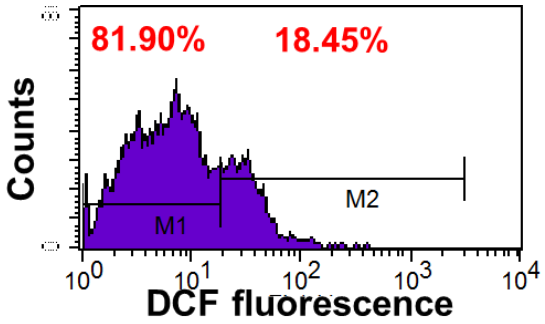

(G) AgNPs-57

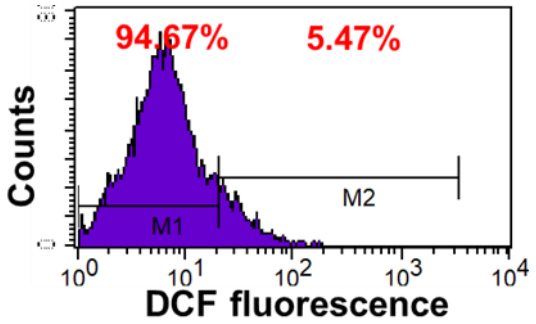

(H)

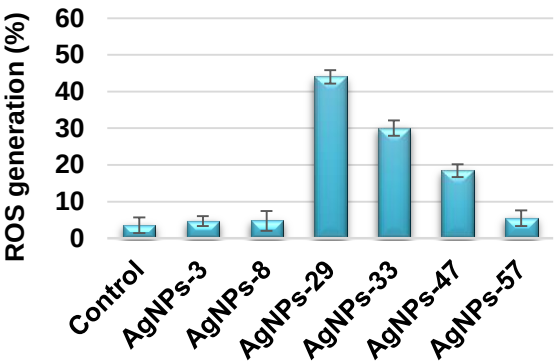

Figure 12.

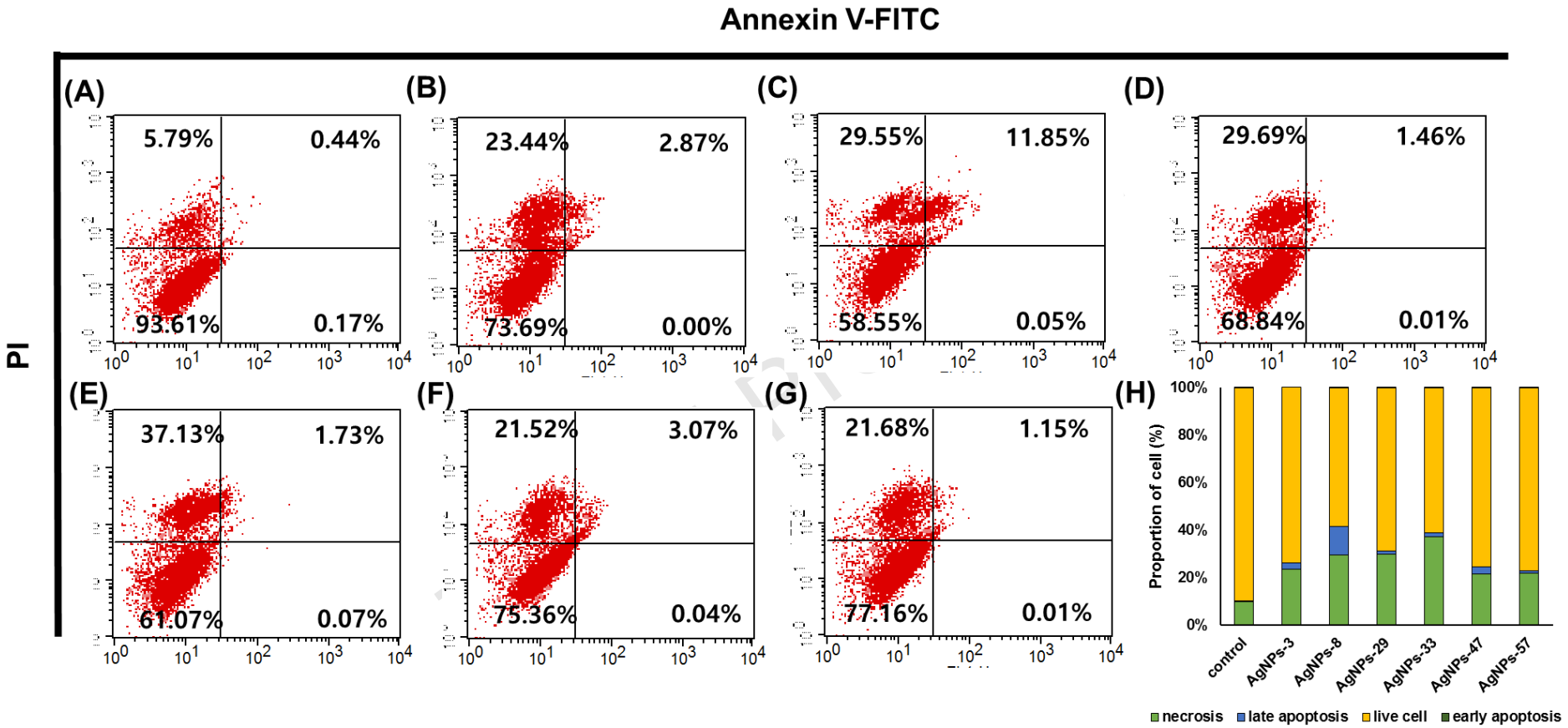
Annexin V-FITC
PI
(A)
5.79%
0.44%
93.61%
0.17%
(B)
23.44%
2.87%
73.69%
0.00%
(C)
29.55%
11.85%
58.55%
0.05%
(D)
29.69%
1.46%
68.84%
0.01%
(E)
37.13%
1.73%
61.07%
0.07%
(F)
21.52%
3.07%
75.36%
0.04%
(G)
21.68%
1.15%
77.16%
0.01%
(H)
Proportion of cell (%)
100%
80%
60%
40%
20%
0%
control
AgNPs-3
AgNPs-8
AgNPs-29
AgNPs-33
AgNPs-47
AgNPs-57
necrosis
late apoptosis
live cell
early apoptosis

Figure 13.

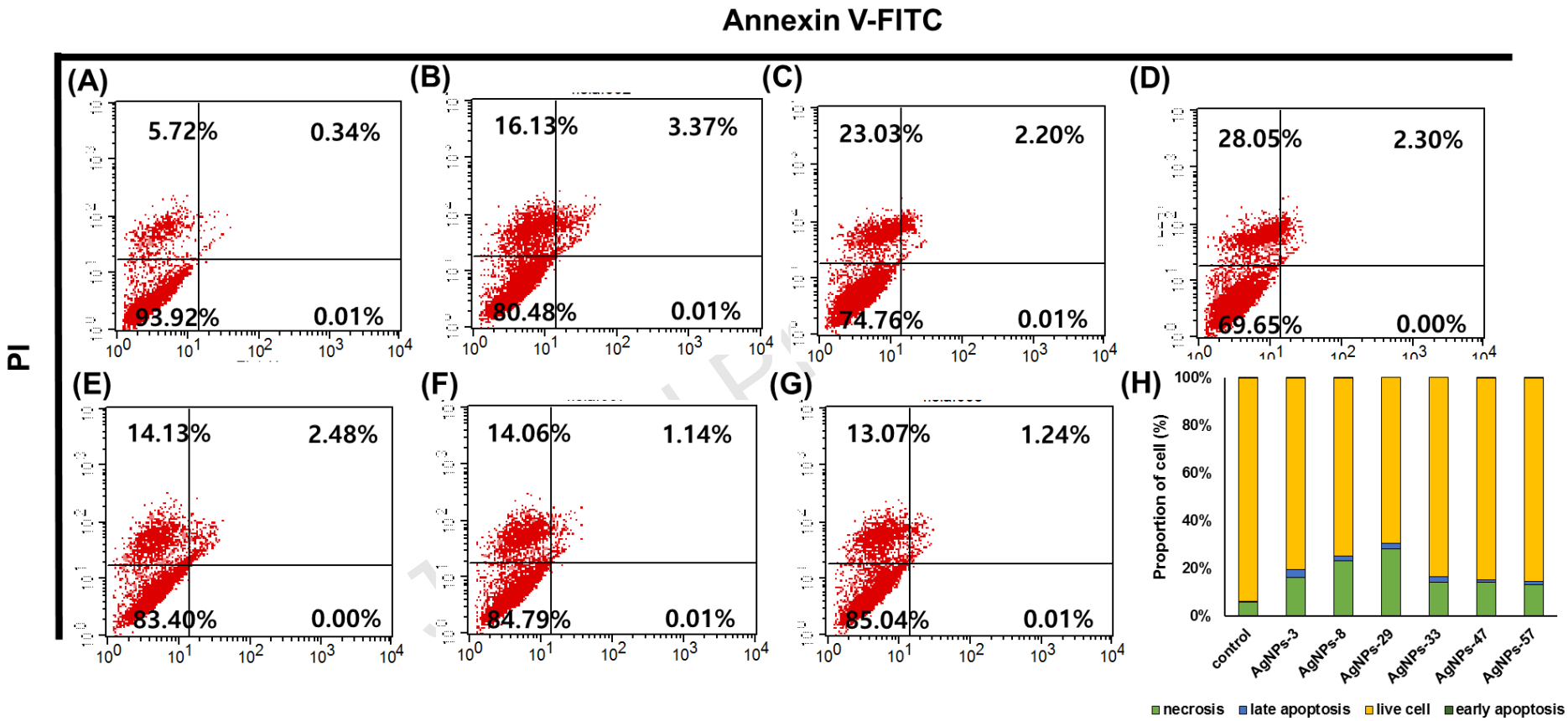
Annexin V-FITC
PI
(A)
5.72%
0.34%
93.92%
0.01%
(B)
16.13%
3.37%
80.48%
0.01%
(C)
23.03%
2.20%
74.76%
0.01%
(D)
28.05%
2.30%
69.65%
0.00%
(E)
14.13%
2.48%
83.40%
0.00%
(F)
14.06%
1.14%
84.79%
0.01%
(G)
13.07%
1.24%
85.04%
0.01%
(H)
Proportion of cell (%)
100%
80%
60%
40%
20%
0%
control
AgNPs-3
AgNPs-8
AgNPs-29
AgNPs-33
AgNPs-47
AgNPs-57
necrosis
late apoptosis
live cell
early apoptosis

Figure 14.

(A) control

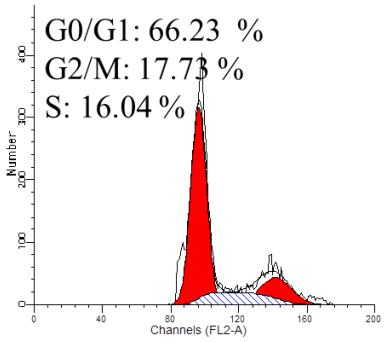

(B) AgNPs-3

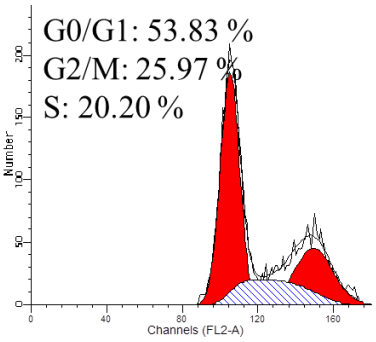

(C) AgNPs-8

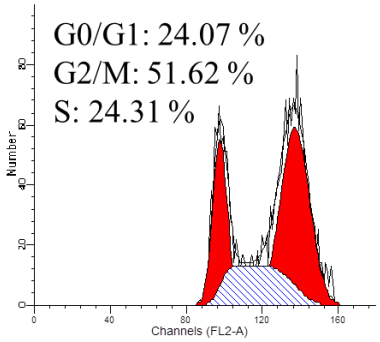

(D) AgNPs-29

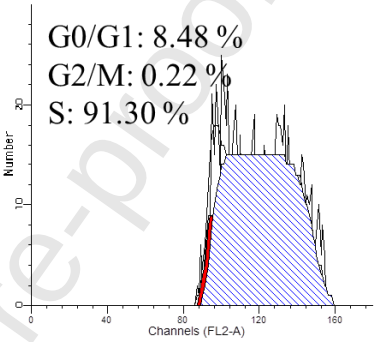

(E) AgNPs-33

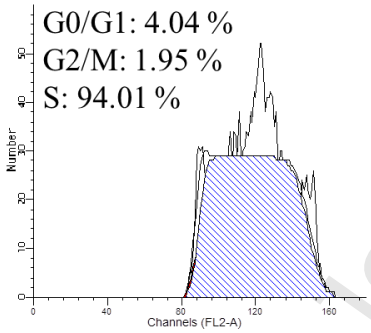

(F) AgNPs-47

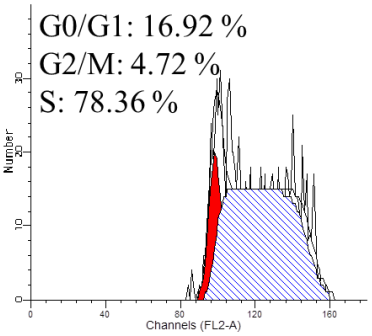

(G) AgNPs-57

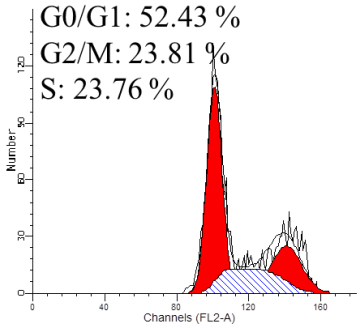

(H)

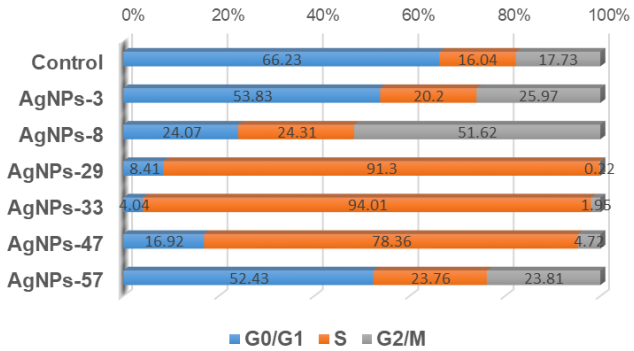

Figure 15.

(A) control

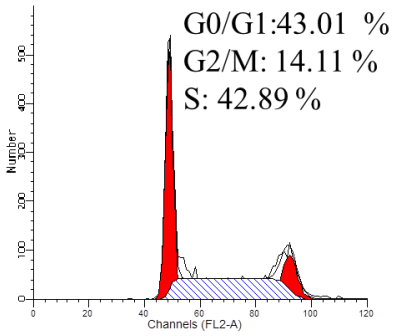

(B) AgNPs-3

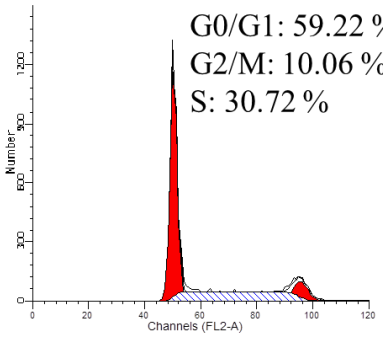

(C) AgNPs-8

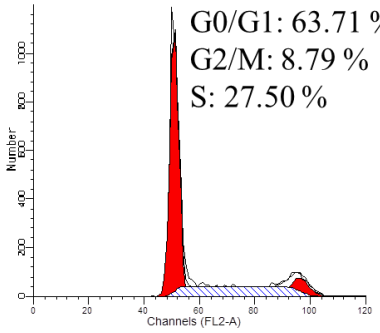

(D) AgNPs-29

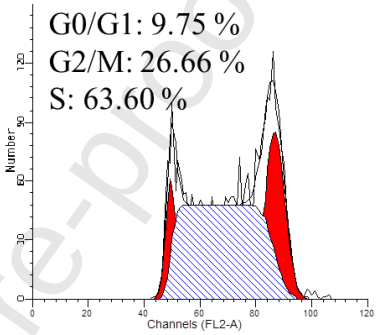

(E) AgNPs-33

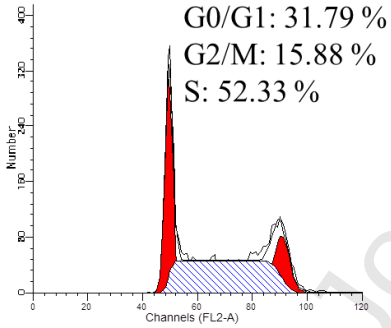

(F) AgNPs-47

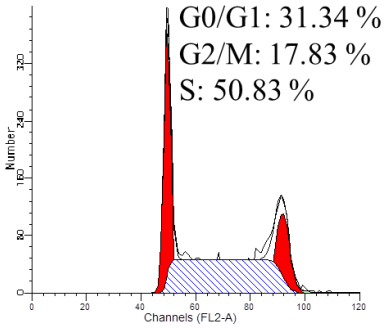

(G) AgNPs-57

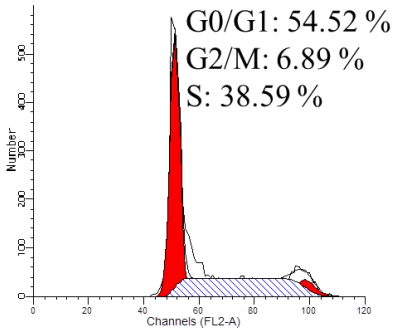

(H)

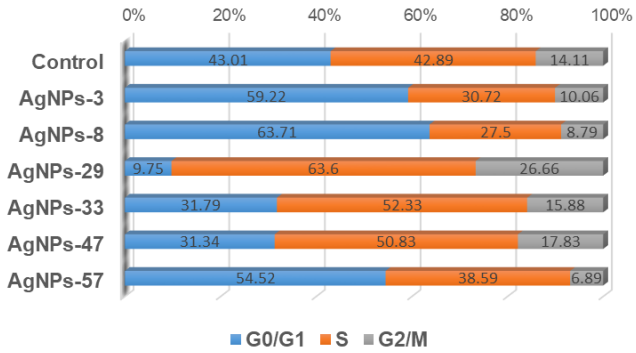

Author Statement

Eun-Young Ahn performed all experimental works. Youmie Park supervised the entire process and drafted the manuscript. All authors read and approved the final manuscript

Declaration of interests

The authors declare that they have no known competing financial interests or personal relationships that could have appeared to influence the work reported in this paper.

Highlights

• Fifty-eight plant extracts are used for green synthesis of silver nanoparticles.

• Synthetic process is totally sustainable and green.

• Silver nanoparticles are cytotoxic and generate ROS in cancer cells.

• Silver nanoparticles induce cell death via mostly necrosis.

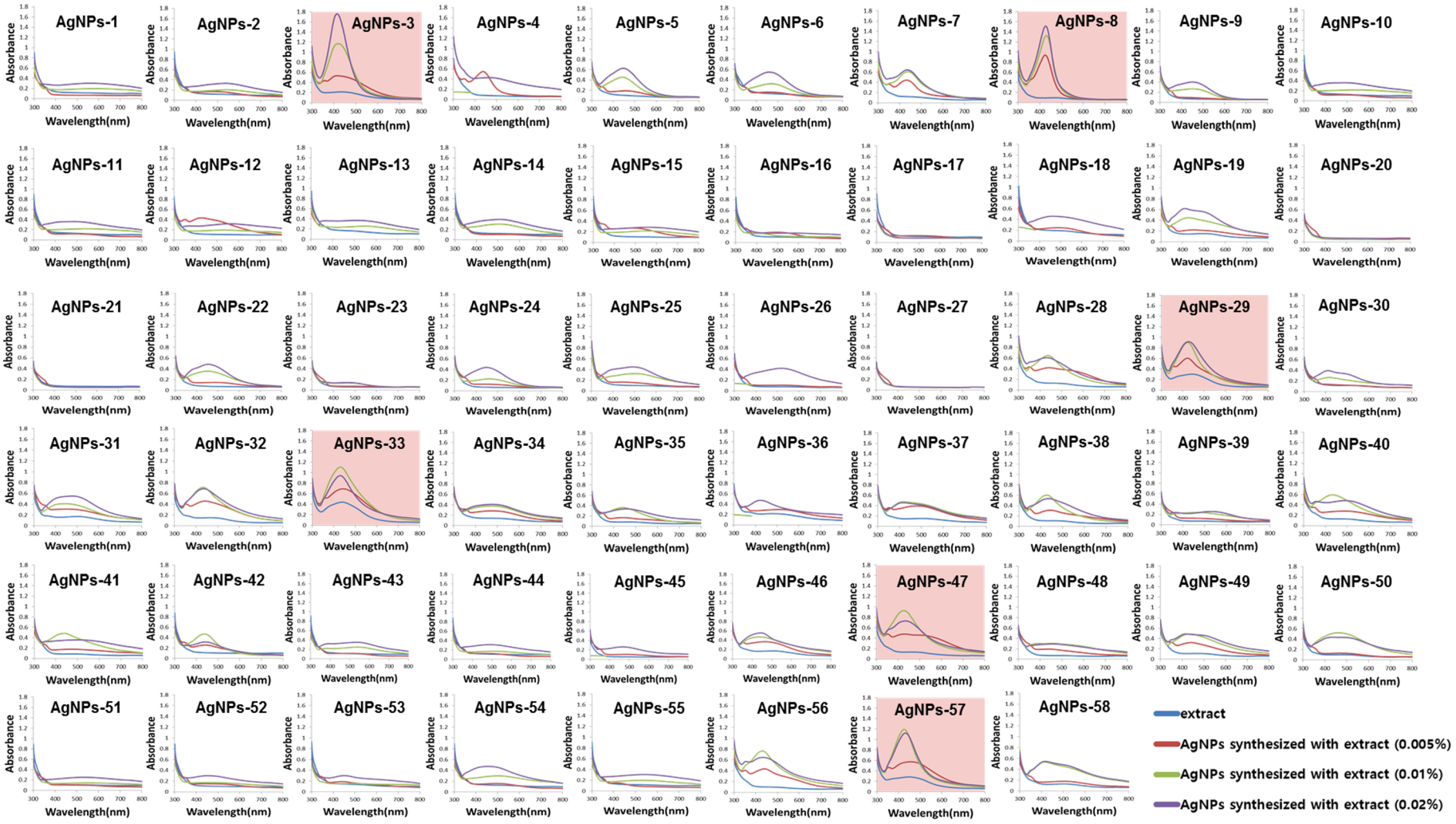
AgNPs-1
AgNPs-2
AgNPs-3
AgNPs-4
AgNPs-5
AgNPs-6
AgNPs-7
AgNPs-8
AgNPs-9
AgNPs-10
AgNPs-11
AgNPs-12
AgNPs-13
AgNPs-14
AgNPs-15
AgNPs-16
AgNPs-17
AgNPs-18
AgNPs-19
AgNPs-20
AgNPs-21
AgNPs-22
AgNPs-23
AgNPs-24
AgNPs-25
AgNPs-26
AgNPs-27
AgNPs-28
AgNPs-29
AgNPs-30
AgNPs-31
AgNPs-32
AgNPs-33
AgNPs-34
AgNPs-35
AgNPs-36
AgNPs-37
AgNPs-38
AgNPs-39
AgNPs-40
AgNPs-41
AgNPs-42
AgNPs-43
AgNPs-44
AgNPs-45
AgNPs-46
AgNPs-47
AgNPs-48
AgNPs-49
AgNPs-50
AgNPs-51
AgNPs-52
AgNPs-53
AgNPs-54
AgNPs-55
AgNPs-56
AgNPs-57
AgNPs-58
Absorbance
Wavelength(nm)
extract
AgNPs synthesized with extract (0.005%)
AgNPs synthesized with extract (0.01%)
AgNPs synthesized with extract (0.02%)

Figure 1

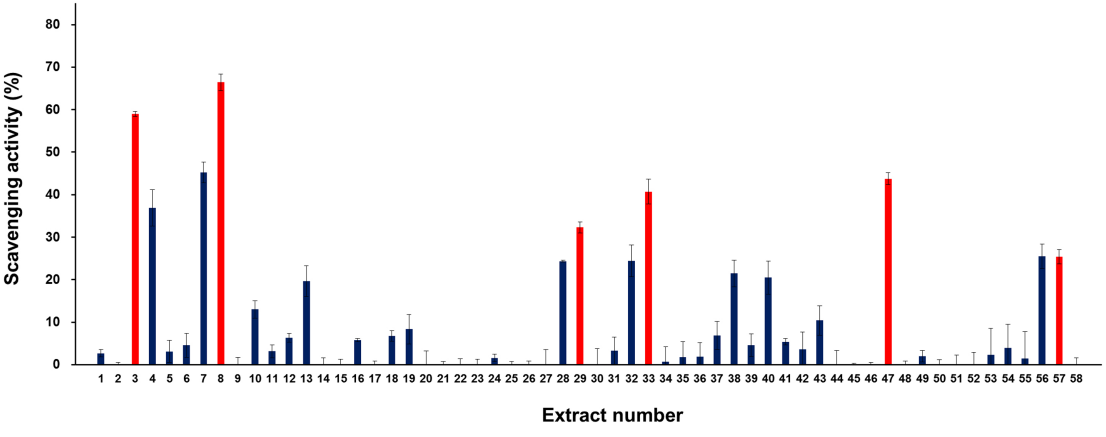
Scavenging activity (%)
0
10
20
30
40
50
60
70
80
1 2 3 4 5 6 7 8 9 10 11 12 13 14 15 16 17 18 19 20 21 22 23 24 25 26 27 28 29 30 31 32 33 34 35 36 37 38 39 40 41 42 43 44 45 46 47 48 49 50 51 52 53 54 55 56 57 58
Extract number

Figure 2

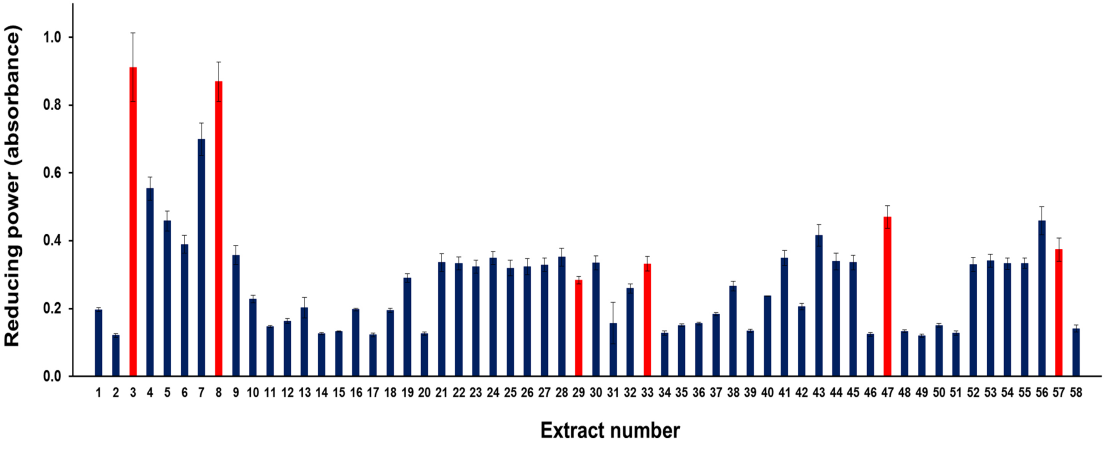
Reducing power (absorbance)
1.0
0.8
0.6
0.4
0.2
0.0
1 2 3 4 5 6 7 8 9 10 11 12 13 14 15 16 17 18 19 20 21 22 23 24 25 26 27 28 29 30 31 32 33 34 35 36 37 38 39 40 41 42 43 44 45 46 47 48 49 50 51 52 53 54 55 56 57 58
Extract number

Figure 3

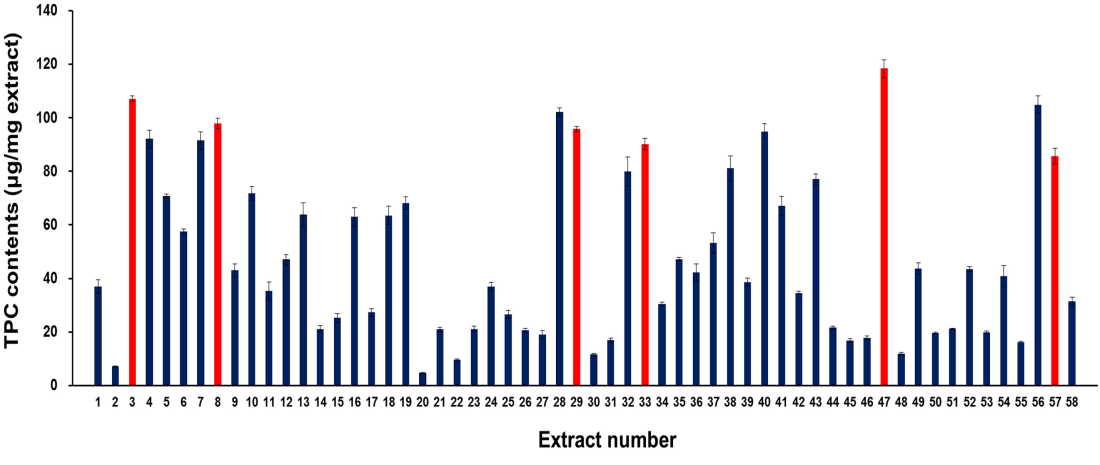
TPC contents (µg/mg extract)
140
120
100
80
60
40
20
0
1 2 3 4 5 6 7 8 9 10 11 12 13 14 15 16 17 18 19 20 21 22 23 24 25 26 27 28 29 30 31 32 33 34 35 36 37 38 39 40 41 42 43 44 45 46 47 48 49 50 51 52 53 54 55 56 57 58
Extract number

Figure 4

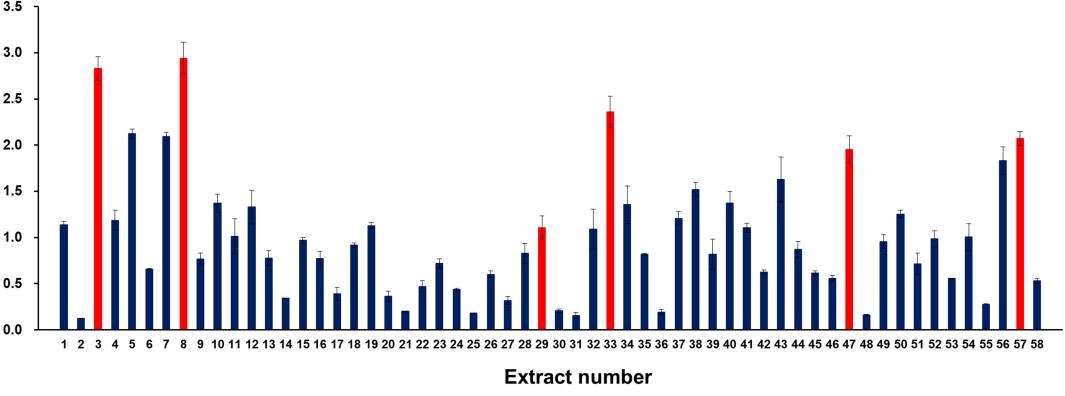
3.5
3.0
2.5
2.0
1.5
1.0
0.5
0.0
1 2 3 4 5 6 7 8 9 10 11 12 13 14 15 16 17 18 19 20 21 22 23 24 25 26 27 28 29 30 31 32 33 34 35 36 37 38 39 40 41 42 43 44 45 46 47 48 49 50 51 52 53 54 55 56 57 58
Extract number

Figure 5

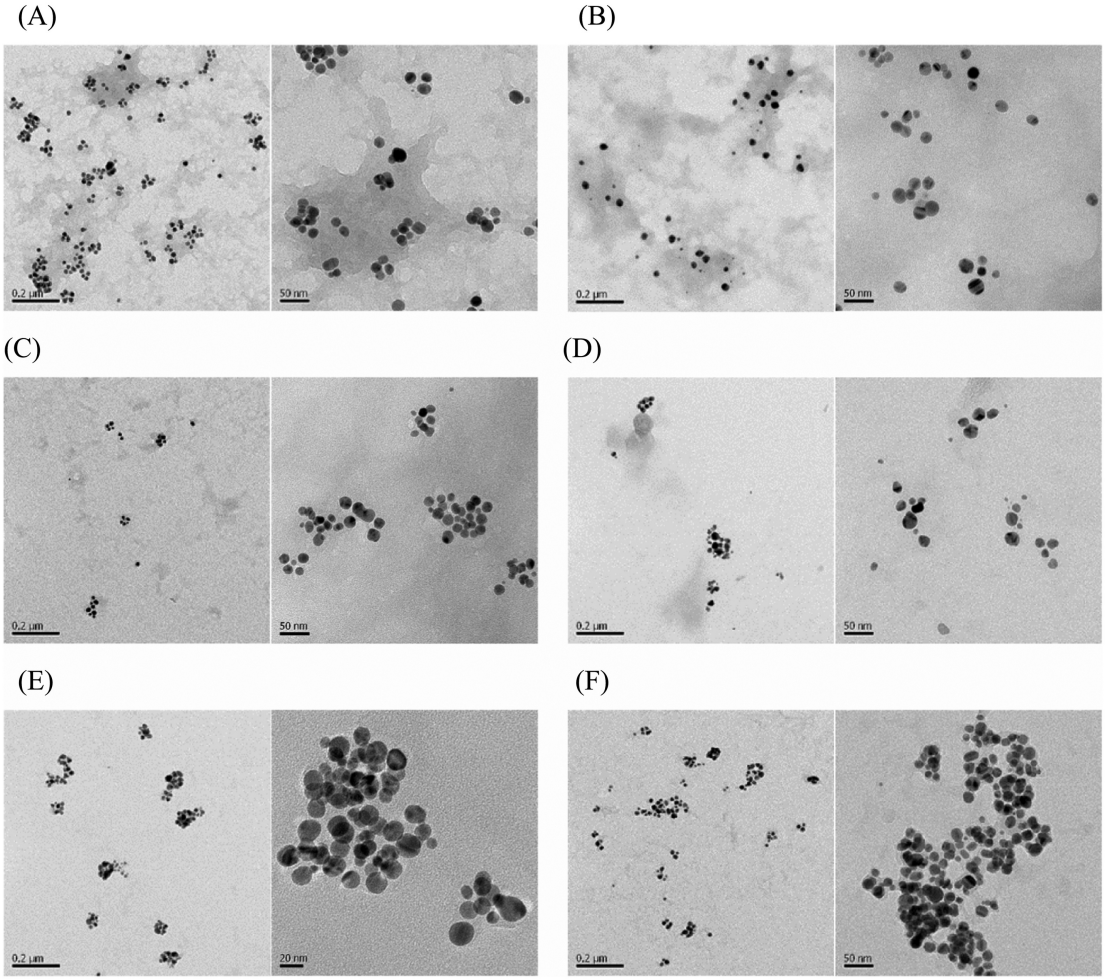
(A)
0.2 µm
50 nm
(B)
0.2 µm
50 nm
(C)
0.2 µm
50 nm
(D)
0.2 µm
50 nm
(E)
0.2 µm
20 nm
(F)
0.2 µm
50 nm

Figure 6

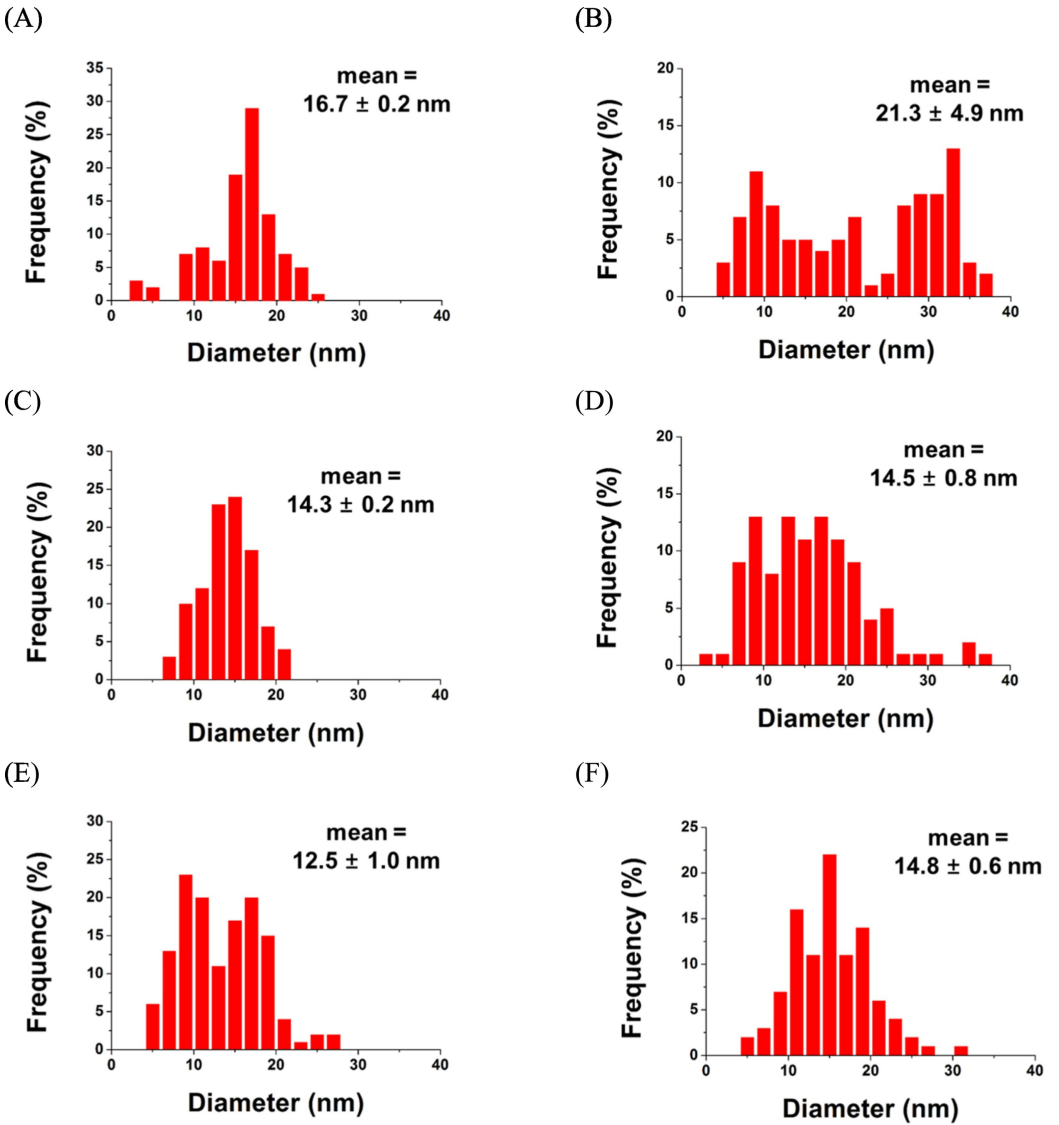
(A)
mean =
16.7 ± 0.2 nm
Frequency (%)
Diameter (nm)
(B)
mean =
21.3 ± 4.9 nm
Frequency (%)
Diameter (nm)
(C)
mean =
14.3 ± 0.2 nm
Frequency (%)
Diameter (nm)
(D)
mean =
14.5 ± 0.8 nm
Frequency (%)
Diameter (nm)
(E)
mean =
12.5 ± 1.0 nm
Frequency (%)
Diameter (nm)
(F)
mean =
14.8 ± 0.6 nm
Frequency (%)
Diameter (nm)

Figure 7

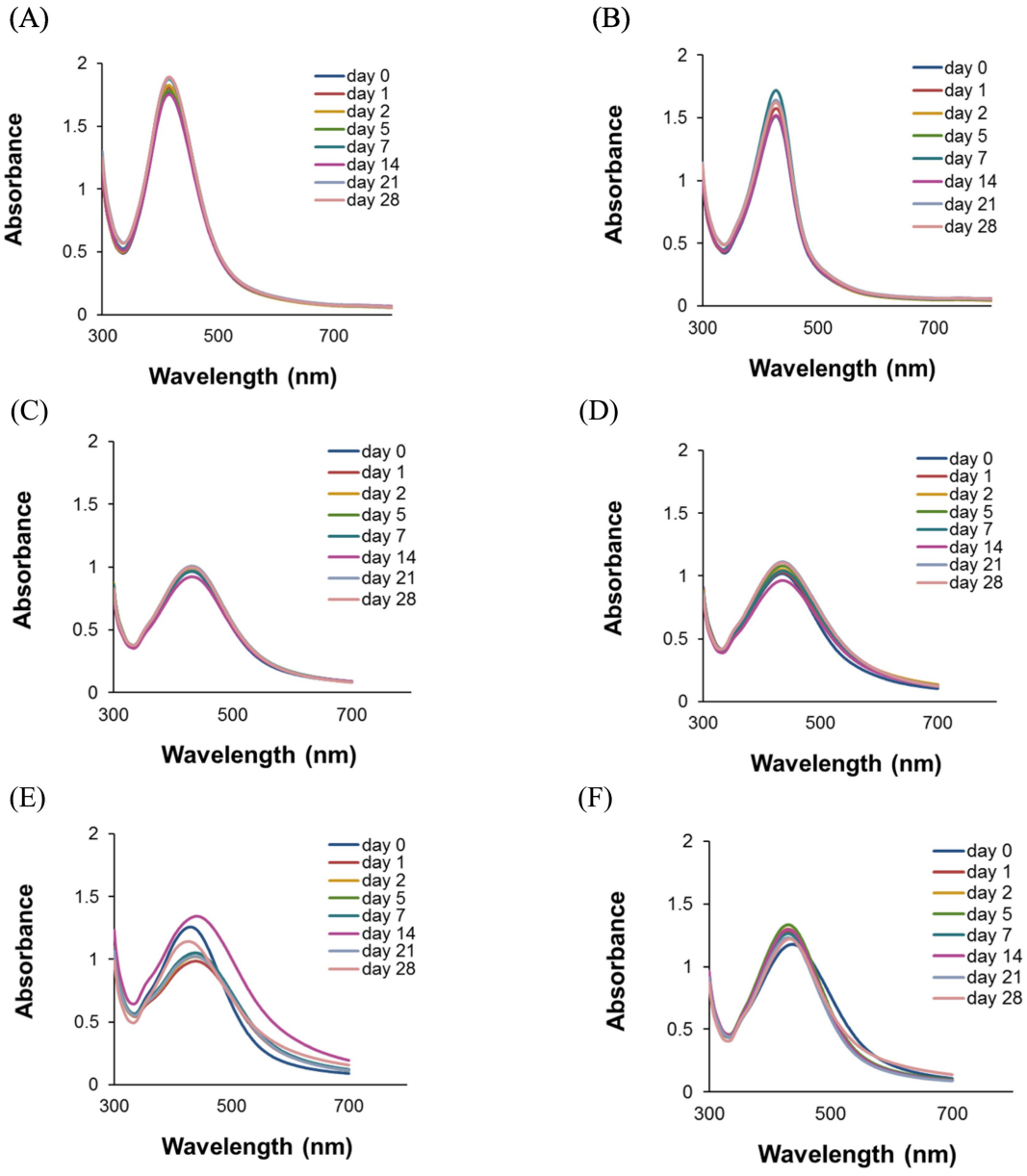
(A)
(B)
(C)
(D)
(E)
(F)
Absorbance
Wavelength (nm)
day 0
day 1
day 2
day 5
day 7
day 14
day 21
day 28
0
0.5
1
1.5
2
300
500
700

Figure 8

(A)

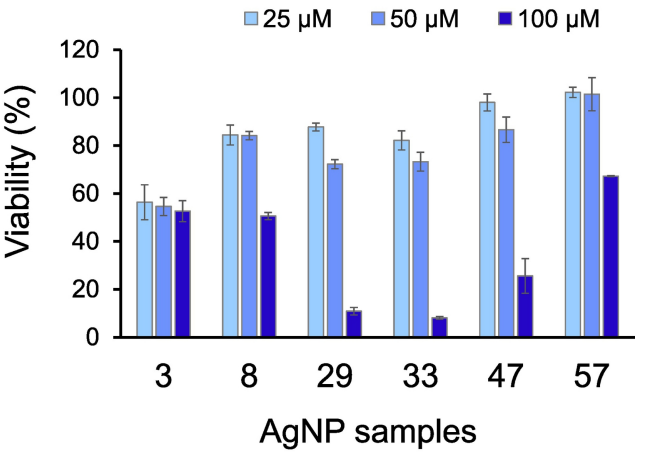
25 µM
50 µM
100 µM
Viability (%)
120
100
80
60
40
20
0
3
8
29
33
47
57
AgNP samples

(B)

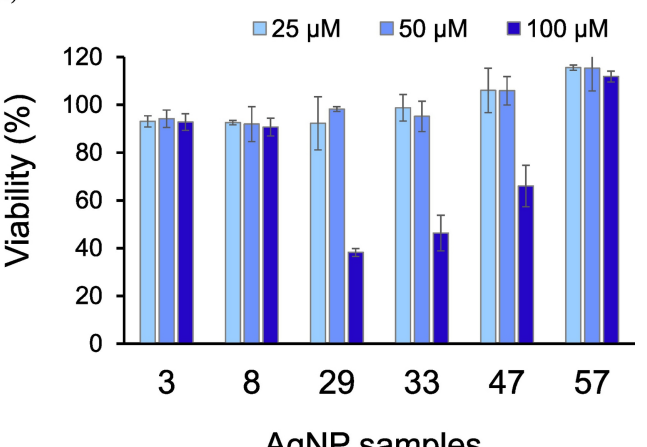
25 µM
50 µM
100 µM
Viability (%)
120
100
80
60
40
20
0
3
8
29
33
47
57
AgNP samples

Figure 9

(A) control

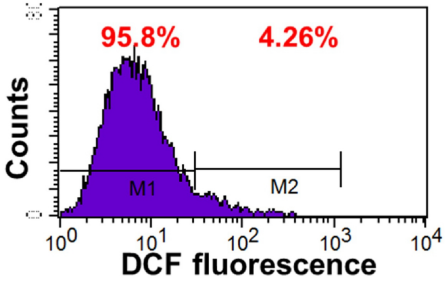

(B) AgNPs-3

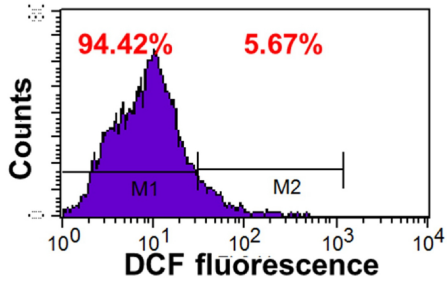

(C) AgNPs-8

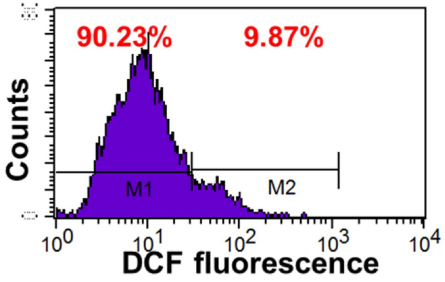

(D) AgNPs-29

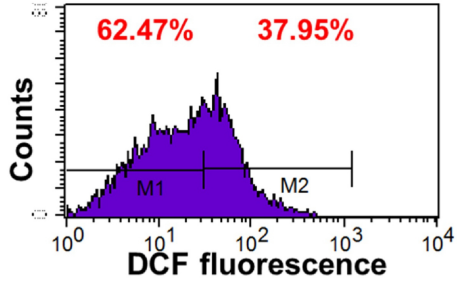

(E) AgNPs-33

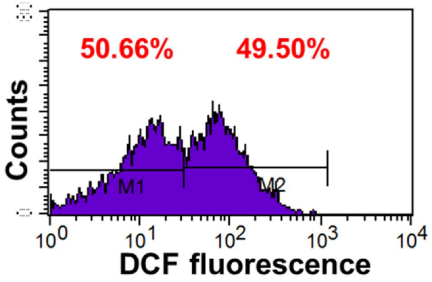

(F) AgNPs-47

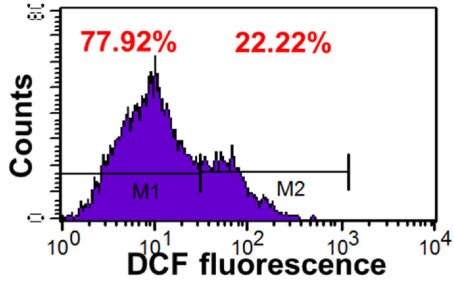

(G) AgNPs-57

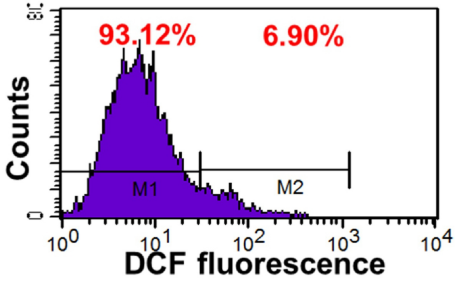

(H)

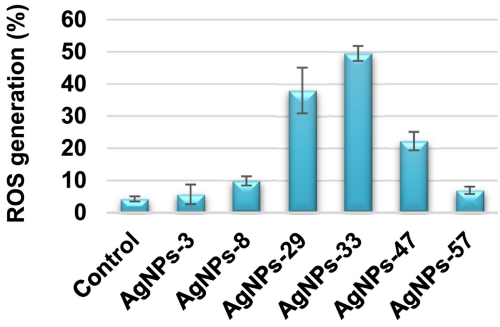

Figure 10

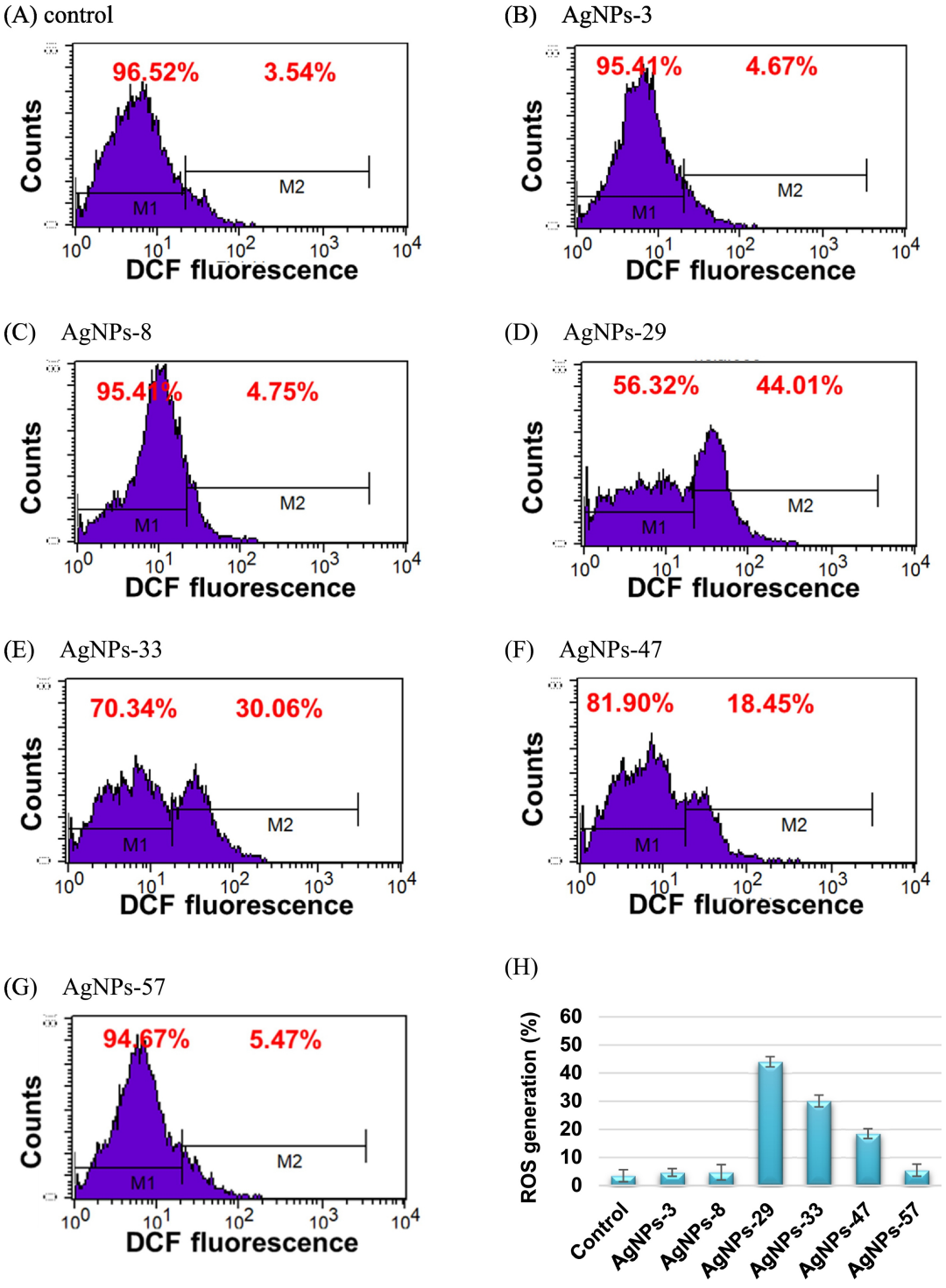
(A) control
96.52%
3.54%
Counts
M1
M2
DCF fluorescence
(B) AgNPs-3
95.41%
4.67%
(C) AgNPs-8
95.41%
4.75%
(D) AgNPs-29
56.32%
44.01%
(E) AgNPs-33
70.34%
30.06%
(F) AgNPs-47
81.90%
18.45%
(G) AgNPs-57
94.67%
5.47%
(H)
ROS generation (%)
0
10
20
30
40
50
60
Control
AgNPs-3
AgNPs-8
AgNPs-29
AgNPs-33
AgNPs-47
AgNPs-57

Figure 11

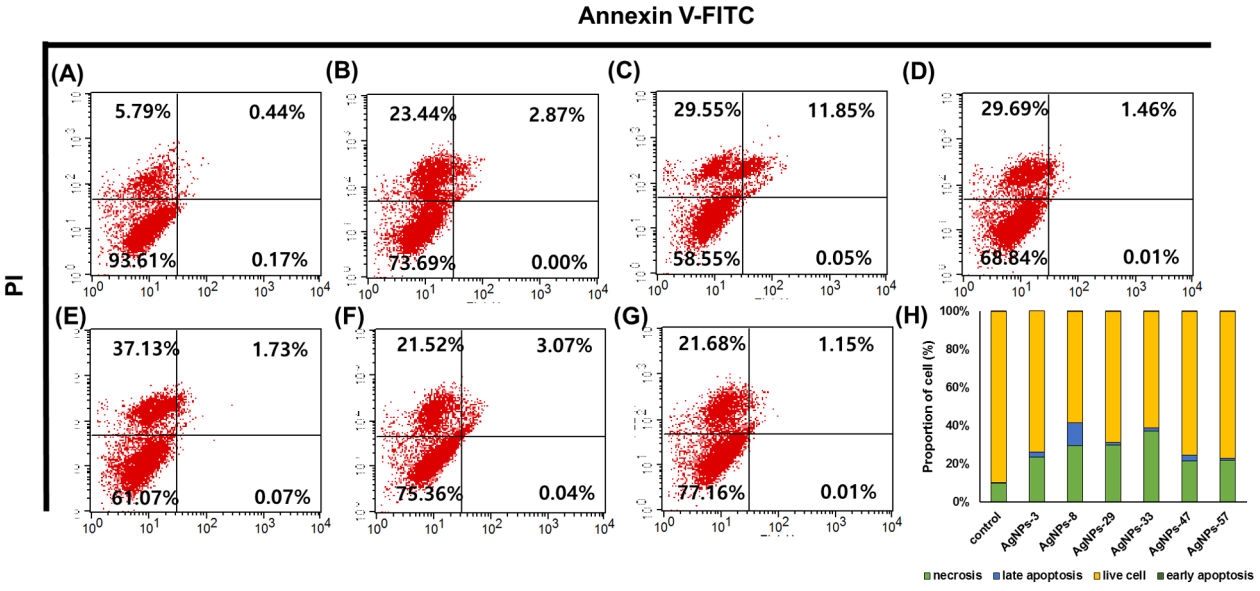
Annexin V-FITC
PI
(A)
5.79%
0.44%
93.61%
0.17%
(B)
23.44%
2.87%
73.69%
0.00%
(C)
29.55%
11.85%
58.55%
0.05%
(D)
29.69%
1.46%
68.84%
0.01%
(E)
37.13%
1.73%
61.07%
0.07%
(F)
21.52%
3.07%
75.36%
0.04%
(G)
21.68%
1.15%
77.16%
0.01%
(H)
Proportion of cell (%)
100%
80%
60%
40%
20%
0%
control
AgNPs-3
AgNPs-8
AgNPs-29
AgNPs-33
AgNPs-47
AgNPs-57
necrosis
late apoptosis
live cell
early apoptosis

Figure 12

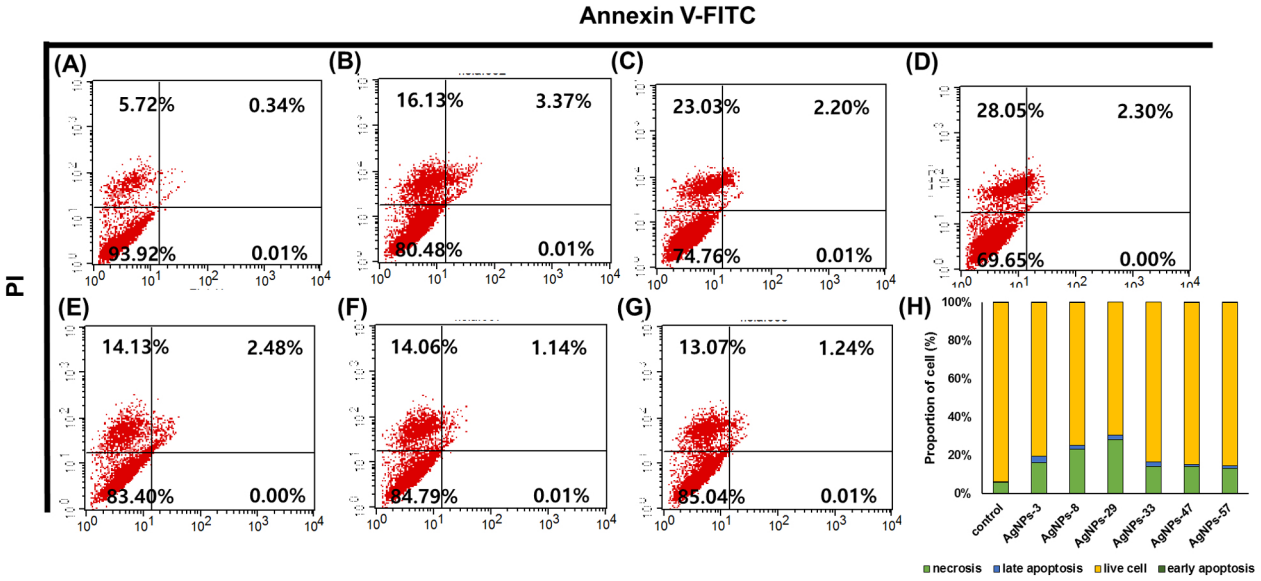
Annexin V-FITC
PI
(A)
5.72%
0.34%
93.92%
0.01%
(B)
16.13%
3.37%
80.48%
0.01%
(C)
23.03%
2.20%
74.76%
0.01%
(D)
28.05%
2.30%
69.65%
0.00%
(E)
14.13%
2.48%
83.40%
0.00%
(F)
14.06%
1.14%
84.79%
0.01%
(G)
13.07%
1.24%
85.04%
0.01%
(H)
Proportion of cell (%)
100%
80%
60%
40%
20%
0%
control
AgNPs-3
AgNPs-8
AgNPs-29
AgNPs-33
AgNPs-47
AgNPs-57
necrosis
late apoptosis
live cell
early apoptosis

Figure 13

(A) control

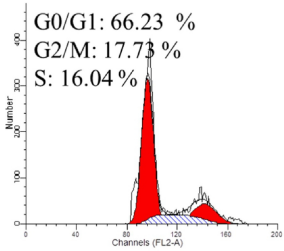

(B) AgNPs-3

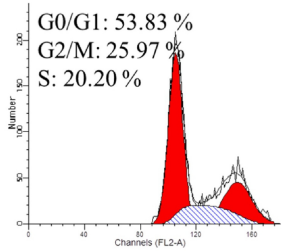

(C) AgNPs-8

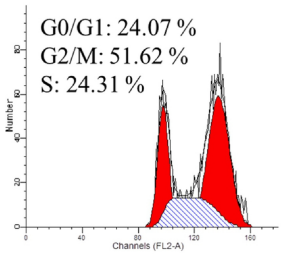

(D) AgNPs-29

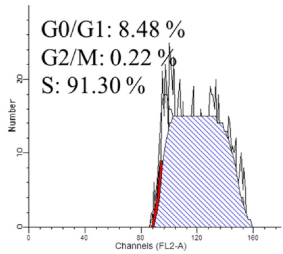

(E) AgNPs-33

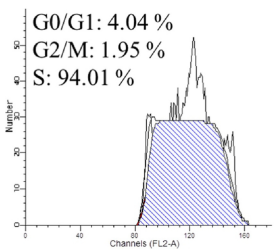

(F) AgNPs-47

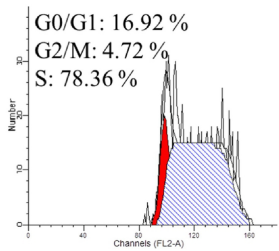

(G) AgNPs-57

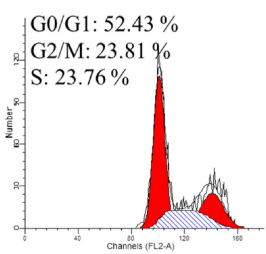

(H)

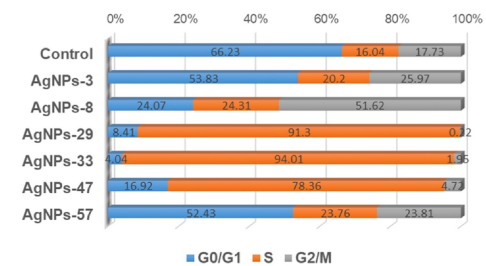

Figure 14

(A) control

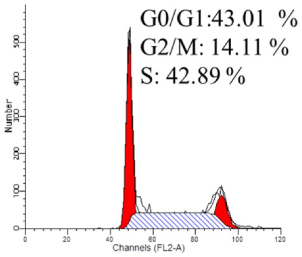

(B) AgNPs-3

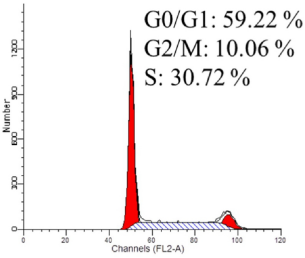

(C) AgNPs-8

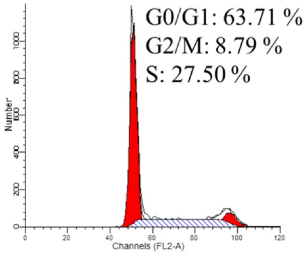

(D) AgNPs-29

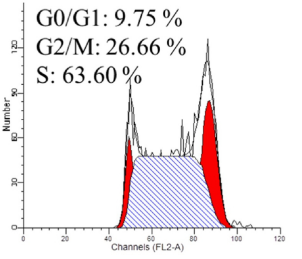

(E) AgNPs-33

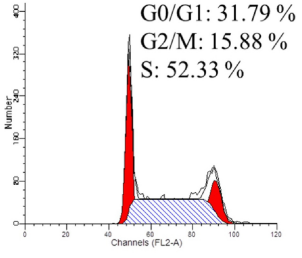

(F) AgNPs-47

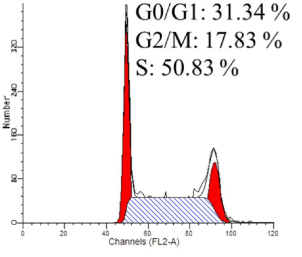

(G) AgNPs-57

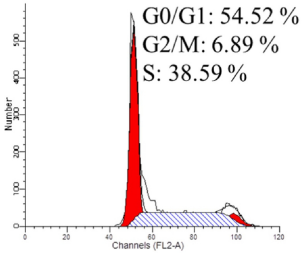

(H)

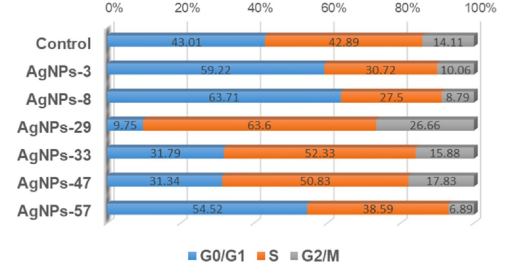

Figure 15